Micron 43 (2012) 1195–1210

Contents lists available at SciVerse ScienceDirect

Micron

journal homepage: www.elsevier.com/locate/micron

In situ ultra-high vacuum transmission electron microscopy studies of the transient oxidation stage of Cu and Cu alloy thin films

Judith C. Yang[a,*], Guangwen Zhou[b]

[a] Department of Chemical and Petroleum Engineering, Department of Physics, University of Pittsburgh, 1249 Benedum Hall, 3700 O'Hara St., Pittsburgh, PA 15261, USA
[b] Department of Mechanical Engineering, State University of New York, PO Box 6000, Binghamton, NY 13902-6000, USA

ARTICLE INFO

Article history:
Received 31 July 2011
Received in revised form 9 February 2012
Accepted 9 February 2012

Keywords:
Oxidation
TEM
In situ
Cu
Cu–Ni
Cu–Au

ABSTRACT

Because environmental stability is an essential property of most engineered materials, many theories exist to explain oxidation mechanisms. Yet, nearly all classical oxidation theories assume a uniform growing film, where structural changes were not considered because of the previous lack of experimental procedure to visualize this non-uniform growth in conditions that allowed for highly controlled surfaces and impurities. With the advent of vacuum technologies and advances in microcopy techniques, especially *in situ*, one can now see structural changes under controlled surface conditions. Here, we present a review of our systematic studies on the transient oxidation stages of a model metal system, Cu, and its alloys, Cu–Au and Cu–Ni, by *in situ* ultra-high vacuum transmission electron microscopy (UHV-TEM). The dependence of the oxidation behavior on the crystal orientation, oxygen pressure, temperature and alloying is attributed to the structures of the oxygen-chemisorbed layer, oxygen surface diffusion, surface energy and the interfacial strain energy. Heteroepitaxial concepts, developed to explain thin film formation on a dissimilar substrate material (*e.g.*, Ge on Si), described well these initial oxidation stages.

1. Introduction

Oxygen in the Earth's atmosphere reacts with metal surfaces forming oxides that are brittle and spall off, leaving bare metal surface for further deterioration. Addressing the problems of corrosion costs the US a few percent of its gross national product (GNP) per year. Fundamental understanding of metal oxidation has therefore received extensive interest owning to its significant technical importance. The general sequence of metal oxidation is oxygen chemisorption, nucleation and growth of oxide, and bulk oxide growth. The oxygen surface chemisorption has been extensively studied by surface science methods that mostly examine the adsorption of up to ~1 monolayer of oxygen with particular emphasis on the structures of adsorbed phases (Besenbacher, 1993, 1996; Jenkins, 2006; Qin et al., 2008; Yagyu et al., 2009; Zhukov et al., 1999). On the other hand, the growth of continuous oxide layer controlled by parabolic, logarithmic, or other kinetic mechanisms at the later stages of oxidation has been observed on many metals systems, and models based on the transport of ionic species through the thicker and continuous oxide film has been proposed to explain the observed trends (Birks and Meier, 1983). Hence, the least well-understood regime in metal oxidation is the transient oxidation stage, *i.e.*, from the nucleation to the growth of metal oxides. Some simple pure metals such as Ni, Al, Cu, and Pb have been selected as model systems to understand the reaction mechanism in the early stages of oxidation by different techniques over a wide range of pressures and temperatures (Brune et al., 1992; Christensen et al., 1986; Holloway and Hudson, 1974; Jacobsen et al., 1995; Kennett and Lee, 1975; Orr, 1962; Thurmer et al., 2002; Vaquila et al., 1993; Yang et al., 1998a,b). The report from these studies that the initial stages of metal oxidation typically involve the nucleation and growth of oxide islands, rather than the formation and thickening of a continuous film, represents a critical departure from previously held assumptions in classic Cabrera–Mott and Wagner theories regarding metal oxidation (Cabrera and Mott, 1948; Wagner, 1933).

To exemplify the structural changes of the initial stages of oxidation and its sensitivity to the environment, we studied the initial oxidation stages of Cu and its alloys by *in situ* UHV-TEM. We selected Cu as the model system, since it has a long history of being studied as a model metal system for oxidation (Cabrera and Mott, 1948; Lawless and Mitchell, 1965; Lawless, 1974; Milne and Howie, 1984; Young et al., 1956). Our study of Cu thin film oxidation was later extended to the cases of Cu–Au(1 0 0) and Cu–Ni(1 0 0) surfaces in order to seek the effects of alloying on the oxide formation (Bharadwaj and Yang, 2001; Luo et al., 2011; Yang et al., 1998a,b,c, 1999,2009, 2002; Yang and Yeadon, 1997; Zhou,

* Corresponding author. Tel.: +1 412 624 8613; fax: +1 412 624 9639.
E-mail addresses: judyyang@pitt.edu, yik3@pitt.edu (J.C. Yang), gzhou@binghamton.edu (G. Zhou).

0968-4328/$ – see front matter © 2012 Elsevier Ltd. All rights reserved.
doi:10.1016/j.micron.2012.02.007

2009a,b,c, 2010; Zhou et al., 2005a,b, 2006,2008; Zhou and Yang, 2002, 2003a,b, 2004, 2005). In this review paper, we first present the oxidation kinetics and oxide morphology from Cu(1 0 0), (1 1 0) and (1 1 1) oxidation as function of temperature and oxidizing pressures (including up to 1 atm), and then compare to the oxidation of Cu–Au(1 0 0) and Cu–Ni(1 0 0). We find these initial stages of oxidation to be a very rich and elegant regime to study. Our studies on the oxidation of Cu thin films demonstrate that oxygen surface diffusion is the primary mechanism of transport, nucleation and growth, in contrast to, for example, bulk diffusion of Cu or oxygen diffusion into the Cu film and oxide nucleation within the film. Since initial stage of oxidation is a surface process, factors that affect the surface impact the oxidation rate and the oxide morphology evolution. A significant effect of temperature is to create different oxide nanostructures, due to temperature-dependent changes in the interfacial strain and properties. This bears a striking resemblance to heteroepitaxy where interfacial strain is the influential factor in thin film growth and nano-shapes. Increasing oxidation pressure shows increased oxidation kinetics, as well as a transition from epitaxial to polycrystalline oxide formation at a critical oxidizing pressure. Alloying dramatically affects both the oxidation kinetics and the morphology of the oxide islands. For Cu–Au oxidation, the oxidation mechanisms change where the Cu_2O reveals a dendritic growth. For Cu–Ni oxidation, the addition of Ni causes the formation Cu_2O and/or NiO where the oxide type(s) and its relative orientation with the film depend on the Ni concentration, oxygen partial pressure and temperature.

2. Materials and methods

Our *in situ* oxidation experiments were carried out in a modified JEOL 200CX TEM (McDonald et al., 1989). This microscope is equipped with a UHV chamber with base pressure $\sim 10^{-8}$ Torr. A controlled leak valve attached to the column of the microscope permits introduction of gases directly into the microscope. Pressure was monitored by an ion gauge mounted inside the column of the microscope near the sample region. Single crystals of Cu(1 0 0), Cu(1 1 0), Cu(1 1 1) as well as Cu–Au(1 0 0) and Cu–Ni(1 0 0) thin films with thickness of 600–1000 Å were grown on single crystal NaCl by sputtering deposition or e-beam evaporation. The films were removed from the NaCl substrate by flotation in deionized water, washed and mounted on a specially designed TEM sample holder that allows for resistive heating at temperatures between room temperature and 1000 °C. The relationship between the power input to the Si TEM sample holder and the temperature was calibrated using a pyrometer. Oxygen gas can be admitted into the column of the microscope through the leak valve at a partial pressure (pO_2) between 5×10^{-5} Torr and 760 Torr. Real time observations can be made at pressures $\leq 8 \times 10^{-4}$ Torr. To investigate the effects of the electron, the electron beam was shut off, the oxidation reaction was carried out for a few minutes, the TEM column was evacuated, and then the electron beam was turned on for imaging. This process was repeated to create a sequential oxidation procedure in order to study the effect of the electron beam on the *in situ* oxidation. The effect of the electron beam is to accelerate the oxidation process but not the morphological developments, thus the mechanisms developed from *in situ* observations are valid and not an electron beam effect.

The Cu, Cu–Au and Cu–Ni films formed a native oxide on the surface due to air exposure. Before oxidation *in situ*, the native oxide of the Cu and the Cu–Au films was reduced inside the TEM by annealing in methanol vapor or Ar plus 2% H_2 environment at 350 °C at a pressure of 5×10^{-4} Torr, as confirmed by selected area electron diffraction (SAD) (Wang et al., 2006; Yang et al., 1998a,b; Zhou et al., 2007a). The Cu–Ni film was reduced by annealing the Cu–Ni films at 750 °C within an Ar plus 2% H_2 atmosphere at a pressure of $\sim 1 \times 10^{-3}$ Torr as was confirmed by SAD (Yang et al., 2009). To oxidize the Cu and Cu alloy films, scientific grade oxygen gas (99.999% purity) was introduced into the TEM chamber.

The Cu–Ni oxidation study also used a controlled environment system constructed for use at the synchrotron X-ray scattering techniques that provide complementary information over a wide range of pO_2 and temperature. Oxidizing and reducing environments are created by mixing purified gases Ar, O_2, CO, CO_2, H_2 and the temperature can achieve up to 1000 °C (Eastman et al., 2005). Epitaxial (0 0 1)Cu_xNi_{1-x} thin film samples with thicknesses of 110–200 nm were grown by electron-beam evaporation onto $SrTiO_3$ single crystal (0 0 1) substrates. The samples were annealed typically for 1 h at 840 °C in 5×10^{-4} Torr of Ar–2% H_2 and then were cooled to the desired temperature for oxidation studies *in situ*.

3. Results and discussion

3.1. Oxidation of Cu

3.1.1. Nucleation and growth of Cu_2O islands on Cu(1 0 0)

Our studies of Cu(1 0 0) oxidation reveal an oxygen surface diffusion as opposed to a Cu or oxygen bulk diffusion mechanism for transport, nucleation and growth of the oxide island. Fig. 1a is a sequence of TEM dark-field (DF) images taken from Cu_2O(1 1 0) reflection, showing the nucleation events of Cu_2O islands in the oxidation of Cu(1 0 0) surfaces at 350 °C and the oxygen pressure of 5×10^{-4} Torr (see Supplemental information for the corresponding *in situ* video). It should be noted that Cu_2O, not CuO, was observed to form under all oxidation conditions studied in this work. Thermodynamically, CuO could only form after a continuous Cu_2O is created, *i.e.*, CuO cannot form directly on Cu; since our focus is on the initial oxidation prior to the oxide scale formation, only Cu_2O was observed in agreement with thermodynamics. After the introduction of oxygen gas, no oxide islands appear within the first couple of minutes; the smallest oxide nuclei observable was ~1 nm. The oxide islands then nucleate rapidly, reach a saturation number density and followed by the island growth. The observation that the number density of oxide nuclei saturates suggests that the nucleation process is limited by oxygen surface diffusion (Yang et al., 1998b), *i.e.*, an active zone of oxygen capture exists around each island, and the radius of this capture zone is proportional to the oxygen surface diffusion rate. The probability of a nucleation event is proportional to the fraction of available surface area outside these zones of oxygen capture. The saturation island density is reached when the zones of oxygen capture of neighboring islands impinge on each other. The equation describing this oxygen surface diffusion behavior for the nucleation of copper oxides:

$$N = \frac{1}{L_d^2}(1 - e^{-kL_d^2 t}) \quad (1)$$

The initial nucleation rate is equal to k, and the saturation island density is $1/L_d^2$. Fig. 1b shows the number density of the oxide islands with respect to the oxidation time, where the solid line corresponds to the fitting to the oxygen surface diffusion limited nucleation processes.

Due to larger surface mobility of oxygen at higher temperatures, the radius of oxygen capture zone increases with temperature and the attachment of oxygen to existing islands is more favorable than nucleation of new nuclei. Therefore, the dependence of the saturation island density, N_S, on oxidation temperature should also follow an Arrhenius relationship (Yang et al., 1998b):

$$N_S \sim e^{E_N/kT} \quad (2)$$

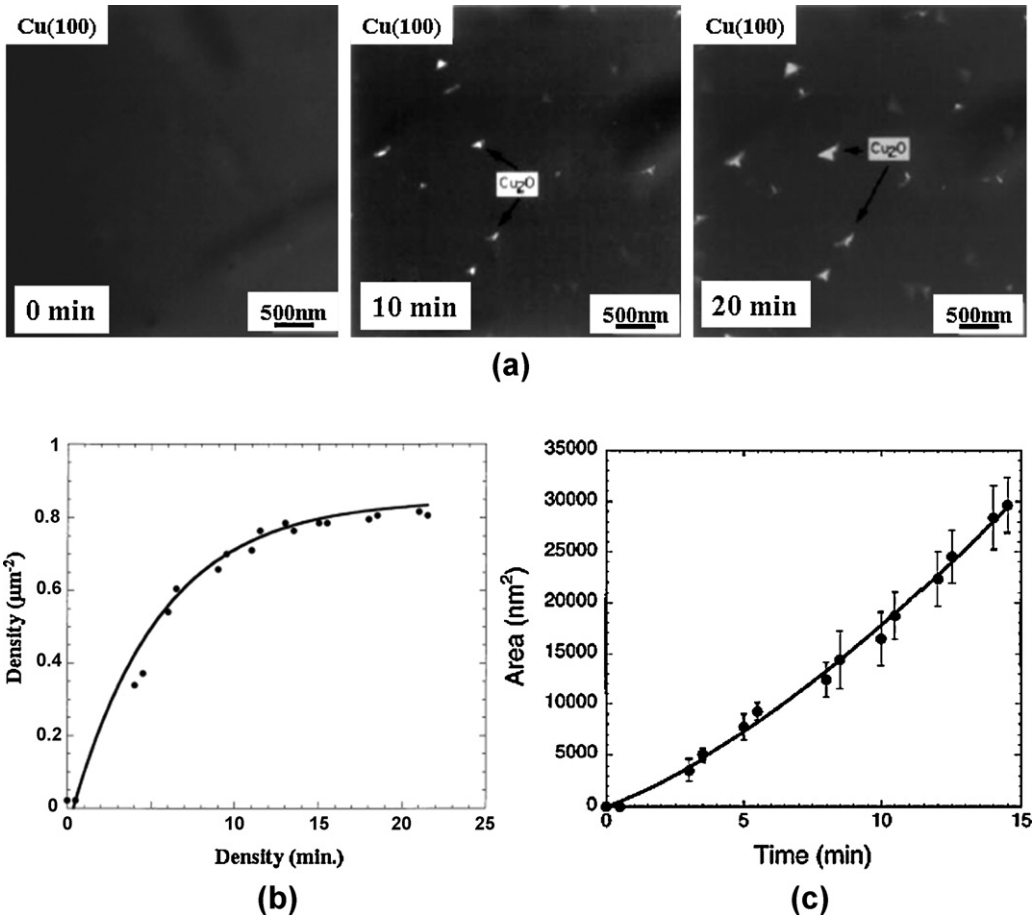

Fig. 1. (a) Cu(2 0 0) dark field image after oxygen is introduced into the microscope at 5×10^{-4} Torr oxygen and 350 °C, (b) nucleation density as function of oxidation time and the solid line is the theoretical fit to an oxygen surface diffusion model, and (c) cross-sectional area of oxide islands which fits a $t^{0.33}$ growth rate where the solid line corresponds to the oxygen surface diffusion/direct impingement model.

where k is Boltzmann constant, T is the temperature, and E_N is the activation energy for the nucleation of oxide islands. It should be noted that this is a homogeneous nucleation model that assumes random selection of nucleation sites. Nearly all of the *in situ* Cu oxidation experiments seem to agree with this assumption, where surface steps (Yang et al., 1999) and dislocations (Zhou et al., 2005b) were not clearly preferential nucleation sites. However if the defects were significant, such as surface faceting, grain boundaries or edge of a hole, then the oxides formed along the defects. For example, Cu(1 1 0) forms surface facets above $T \simeq 750$ °C, where the oxide grew as nanorods along the valleys of the facets (Zhou et al., 2005b).

The evolution of individual islands during growth can also be followed *in situ*. Fig. 1c shows the quantitatively measured island areas as a function of oxidation time when Cu(1 0 0) is exposed to an oxygen pressure of 5×10^{-4} Torr at 350 °C. The best power law fit to the island growth is $t^{1.3}$, which is slightly higher than t—the predicted power law dependence for 3D growth by oxygen surface diffusion (Yang et al., 1997). To account for the slight deviation from the linear growth, we included the direct impingement or bulk diffusion of oxygen that contributes to the island growth, which fits with the experimental data (Yang et al., 1997), as shown in Fig. 1c. Hence, these *in situ* studies of Cu oxidation revealed that oxygen surface diffusion is the primary mechanism of transport, nucleation and growth during the initial oxidation stage; as the oxide islands grow larger, the oxygen atoms that land on the surface of the oxide island also contribute to its growth.

3.1.2. *Effect of surface orientation on the oxide formation: oxidation of Cu(1 1 0) and Cu(1 1 1)*

Previous investigators have elegantly demonstrated that Cu(1 0 0) and (1 1 0) surfaces are unreconstructed, and then transform into "missing-row" or "adding-row" reconstruction when exposed to oxygen (Jacobsen and Norskov, 1990; Jensen et al., 1990; Robinson et al., 1990). After reconstruction, oxygen diffuses on the reconstructed surface, and nucleation occurs on the reconstructed Cu–O surface. Further arriving oxygen can either nucleate new oxide islands by reacting with copper atoms or attach to an existing island, causing growth. Therefore, the surface diffusion coefficient of oxygen may determine the outcome of the competition between nucleation and growth, and, hence, determines the number density of stable islands. Qualitatively a larger diffusion coefficient for oxygen should yield a lower number density of stable islands. Since the path length of oxygen surface diffusion depends on the atomic structure of the substrate plane, different nucleation behaviors of Cu_2O islands is therefore expected for different orientations of the Cu. The Cu(1 0 0) has a more close-packed structure, and is smoother than the corrugated Cu(1 1 0) surface. Similarly, the reconstructed $(\sqrt{2} \times 2\sqrt{2})R45^\circ$ O–Cu(1 0 0) surface has a more compact oxygen chemisorption than (2×1)O–Cu(1 1 0) surface which has a corrugated structure. Therefore, it is expected the activation barrier of surface diffusion of the dissociated oxygen be higher on the Cu(1 1 0) surface, and thus have a shorter path length. The shorter diffusion path length leads to a smaller zone of oxygen capture. If an adatom lands within the zone of

Table 1
Comparison of the nucleation kinetics in the oxidation of Cu(1 0 0) and Cu(1 1 0) at 350 °C and oxygen pressure of 5×10^{-4} Torr.

	Initial nucleation rate (k: μm^{-2} min^{-1})	Radius of oxygen capture zone (L_d: μm)	Saturation island density ($1/L_d^2$: μm^{-2})	Island density saturation time (min)	Nucleation activation energy (E_a: eV)
Cu(1 0 0)	0.17	1.09	0.83	22	1.4 ± 0.2
Cu(1 1 0)	1.743	0.33	9.01	17	1.1 ± 0.2

oxygen capture, then adatom will diffuse on the surface and attach to an existing island; an adatom landing outside this zone of oxygen capture could create its own nucleation site. The smaller zone of oxygen captures results in a higher number density of oxide nuclei. This is confirmed by our results where the active zone of oxygen capture around each island on Cu(1 1 0) is 0.3331 μm for the oxidation at 350 °C, which is significantly smaller than that on Cu(1 0 0), 1.09 μm, as shown in Table 1.

Rather than following the process of nucleation and growth of oxide islands as described earlier for Cu(1 0 0) and Cu(1 1 1), the oxidation of Cu(1 1 1) shows a very different behavior. As seen in Fig. 2, the oxidation of Cu(1 1 1) surface is *via* the nucleation and growth of "discontinuous-branched" Cu_2O overlayer under similar oxidation condition ($T = 450$ °C $pO_2 = 5 \times 10^{-4}$ Torr). Further oxidation results in growth of these Cu_2O islands where they coalesce to create irregularly connected oxide clusters. With use of a connectivity-checking algorithm, individual Cu_2O clusters can be isolated for statistical analysis, as shown in Fig. 2a–c (Zhou et al., 2008). Under the scaling hypothesis, the infinite cluster at the percolation threshold p_c has the property of statistical self-similarity, which can be checked by measuring the mass $M(L)$ of the infinite cluster and that of the backbone with different length scale L. At the percolation threshold, $p = p_c$, the mass of the spanning cluster scales with L as (Fender, 1988; Stauffer, 1979):

$$M(L) = L^D f\left(\frac{L}{\xi}\right) \rightarrow \begin{cases} L^D \text{ for } L \gg \xi \\ L^E \text{ for } L \gg \xi \end{cases} \quad (3)$$

Here ξ is the correlation length defined as the average root mean square distance between occupied sites that belong to the same cluster, D is the fractal dimension of the cluster, and E is the Euclidean dimension where $E = 2$ for a two-dimension surface. As shown in Fig. 2d, the mass densities for the infinite cluster are scale dependent, follow the power law in Eq. (3) with the $L \ll \xi$, and have the fractal dimension of $D = 1.71$. The fractal dimension $D = 1.71$ of the infinite oxide cluster is inconsistent with the prediction by random percolation, which gives $D = 1.9$. We speculate such a random site occupation mechanism does not apply to metal oxidation, where the oxide nuclei attract oxygen atoms for the oxide growth. This implies that the probability of site occupation is neighbor dependent for surface oxidation, and sites adjacent to the periphery of existing oxide have larger probability to be occupied. We use kinetic Monte-Carlo (KMC) simulations to verify the above speculation (Fig. 2e), where the probability for oxygen atoms being captured by existing oxide islands is larger than the nucleation of new islands due to the smaller activation energy for an oxygen atom sticking to an existing oxide island. Our KMC simulations reveal a fractal dimension of $D = 1.75$ with $L \ll \xi$ (Fig. 2f), which is very close to the experimental fractal dimension ($D = 1.71$) of the infinite oxide cluster observed experimentally. Their agreement supports our speculation that the percolating oxide film growth during Cu(1 1 1) oxidation is related to the processes of neighbor-dependent site occupation of oxygen and supports our nucleation model of an oxygen capture zone around existing islands.

One might expect that the mechanism of neighbor-dependent site occupation is typical for oxide growth during metal oxidation. This implies that percolating oxide film growth could be a general phenomenon for metal oxidation. However, our *in situ* TEM observations of the oxidation of Cu(1 0 0), Cu(1 1 0) and Cu(1 1 1) under similar oxidation conditions reveal that the oxidation of Cu(1 0 0) and (1 1 0) leads to the formation of 3D compact Cu_2O islands (Zhou and Yang, 2002, 2003a,b, 2004; Zhou et al., 2005a), which obviously deviates from the fashion of percolating oxide growth. These different oxidation behaviors can be attributed to their different oxygen chemisorbed structures. The O-chemisorption on Cu(1 1 1) results in ordered '29' ($\sqrt{13}R46.1° \times 7R21.8°$) and '44' ($\sqrt{73}R5.8° \times \sqrt{21}R - 10.9°$) lattice structures, which comprise distorted hexagonal arrays of O atoms with unit cell areas 29 and 44 times larger than that of the substrate Cu(1 1 1) (Besenbacher and Norskov, 1993; Jensen et al., 1991, 1991, 1992; Matsumoto et al., 2001). The oxygen atoms in the 29 and 44 structures have more than one well-defined height with corrugation up to ~3.1 Å with respect to the Cu surface. Compared to the chemisorbed structures of ($\sqrt{2} \times 2\sqrt{2}$) R45° O–Cu(1 0 0) and ($2 \times 1$)O–Cu(1 1 0), the oxygen-chemisorbed '29' and '44' structures on Cu(1 1 1) surfaces have much larger surface corrugation, and such enhanced surface roughness can greatly inhibit surface diffusion of oxygen atoms. Efficient surface and edge diffusion usually leads to compact island growth, while sluggish surface diffusion causes ramified island morphologies. The percolating oxide growth during Cu(1 1 1) oxidation can be attributed to the restricted surface diffusion of oxygen due to the highly corrugated O–Cu(1 1 1) surface structure, and the compact oxide island growth observed during the oxidation of O–Cu(1 0 0) and O–Cu(1 1 0) surfaces is related to the efficient oxygen surface diffusion due to their smooth surface structures.

3.1.3. *Effect of oxidizing temperature on the oxide morphology*

We systematically investigated the role of oxidizing temperature and pressure, where we discovered an unusually wide variety of oxide nanostructures, from nanorods to pyramids to a nearly uniform oxide layer, by simply changing the oxidation temperature (Fig. 3). These *in situ* studies also provide insights into nano-oxide synthesis. Similar to heteroepitaxy, the lattice mismatch causes different nanostructures; different shapes are noted including thin films, domes or nanorods where the common explanation is the strain between the thin film and support material (Ross et al., 1998, 1999; Tersoff and Tromp, 1993; Tromp and Ross, 2000). We find in this case that strain does indeed play a critical role in defining these shapes. The temperature impacts surface and interface energies as well as mechanical properties, which affect the oxide morphology. Two of the unusual shapes—the nanorod (Zhou and Yang, 2002) and the hollow pyramid (Zhou et al., 2005a)—were of particular interest and studied in detail.

3.1.3.1. Cu_2O nanorods. Elongated Cu_2O islands were observed to form on Cu(1 0 0) surfaces from the *in situ* oxidation in a narrow temperature regime near 600 °C (Zhou and Yang, 2002, 2003b). The island initially has a square-in-cross-section shape and when a critical size (~110 nm), is reached, the island transitioned to an elongated structure (Fig. 4a). These shapes bear a striking resemblance to nanorods observed in a few heteroepitaxial systems such as Ge nanorods on Si. Tersoff and Tromp (1993) have proposed an energetic model to describe square-elongation shape transition of epitaxial islands. According to their model, the energy per unit

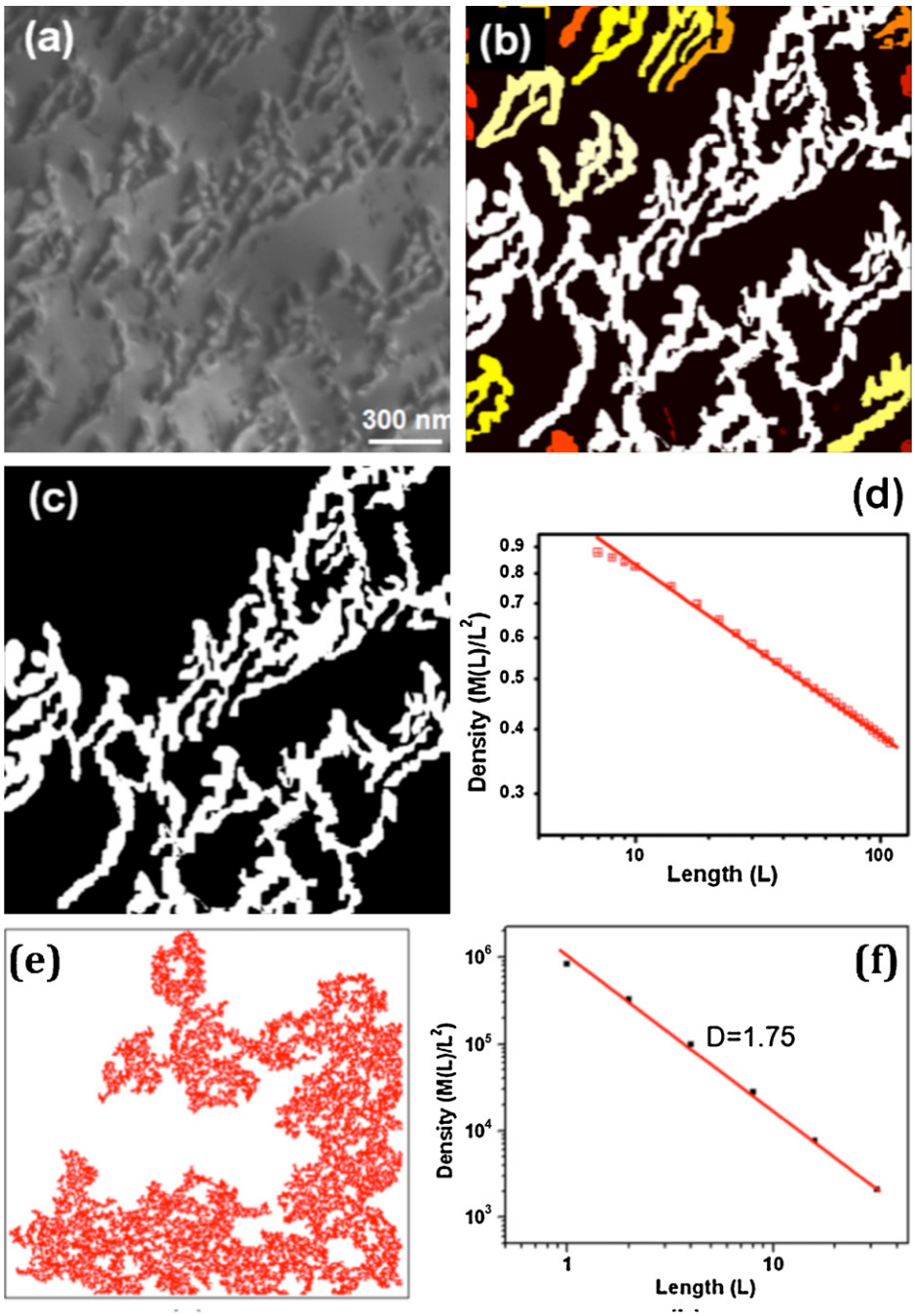

Fig. 2. The Cu_2O formed on the Cu(1 1 1) film at the percolation threshold: (a) identification of oxide clusters by a connectivity analysis of the discontinuous oxide film, different clusters are shown by different colors, and the largest one (infinite cluster) has the brightest contrast and spans over the whole image; (b) the infinite cluster singled out from (a). (c) Scaling analysis of the infinite cluster, (d) log–log plot of $M(L)/L^2$ *vs.* L for the infinite cluster, the fraction dimension D for the infinite cluster is determined to be 1.71. Note that L is the number of pixels of the image and can be converted into length scale by $L(\text{nm}) = L(\text{pixel number}) \times (\text{image size(nm)}/1024)$. (e) The infinite cluster formed at the percolation threshold from the KMC simulations based on the neighbor-dependent site occupation mechanism; (f) log–log plot of $M(L)/L^2$ *vs.* L for the infinite cluster, the fraction dimension D for the infinite cluster is determined to be 1.75 (L is the number of pixels).

volume (E/V) of a strained epitaxial island is:

$$\left\{ \frac{E}{V} = 2\Gamma\left(\frac{1}{s}+\frac{1}{t}\right) + \frac{1}{h}(r_i + r_t - r_s) \right.$$
$$\left. -2ch\left[\frac{1}{s}\ln\left(\frac{se^{3/2}}{h\cot\theta}\right) + \frac{1}{t}\ln\left(\frac{te^{3/2}}{h\cot\theta}\right)\right], \right\} \quad (4)$$

where s, t, and h are the width, length, and height of the island, respectively; θ being the contact angle. Γ contains the surface and interface energies and contact angle, $\Gamma = \gamma_e \csc\theta - (\gamma_t + \gamma_s - \gamma_i)\cot\theta$ (units J/m^2); γ_t, γ_s, and γ_e are the surface energies (per unit area) of the island's top, the substrate, and the island's edge facet, respectively; γ_i is the island-substrate interface energy. The first two terms in Eq. (4) give the change in surface and interface energies when an island forms on the surface. The substrate-island lattice mismatch causes the island to exert a force on the substrate, which elastically distorts the substrate. The third term describes the energy relaxation of the island by the cost of some strain in the substrate, and this relaxation energy is related to c, $c = \sigma_b^2(1-\nu)/2\pi G$, where ν and G are the Poisson ratio and shear modulus of the substrate, and σ_b is the island bulk stress (Tersoff and LeGoues, 1994; Tersoff and Tromp, 1993).

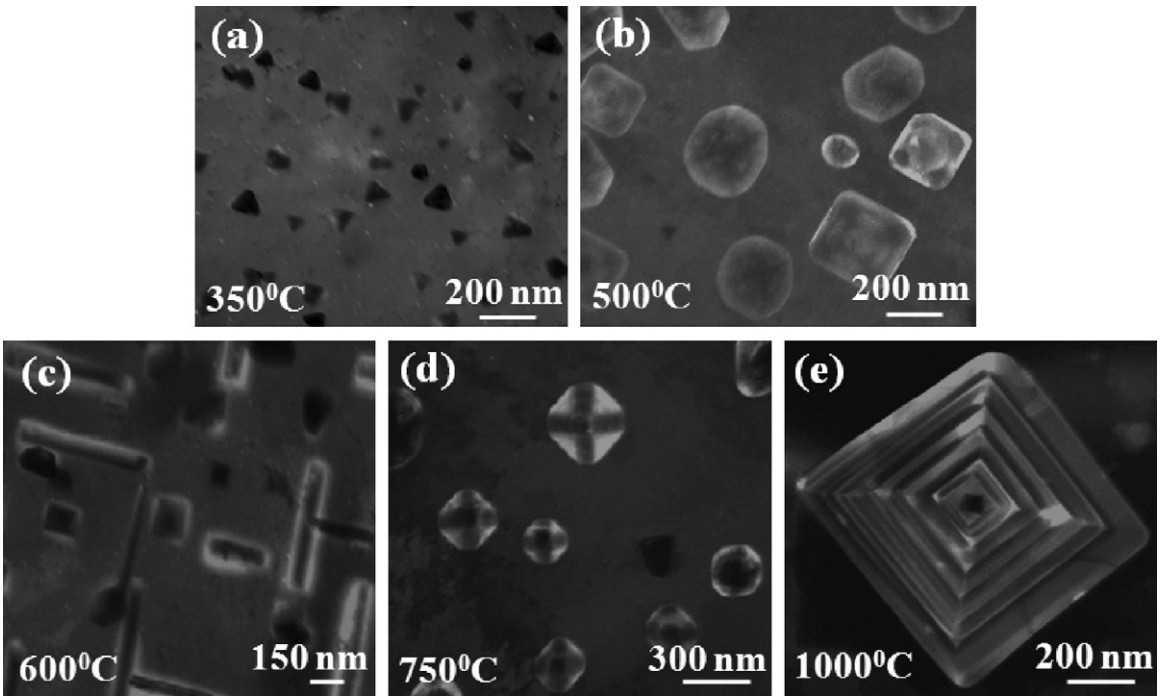

Fig. 3. The morphology of Cu_2O islands formed on Cu(1 0 0) surface as a function of oxidation temperature: (a) 350 °C, (b) 500 °C, (c) 600 °C, (d) 750 °C, and (e) 900 °C, where oxygen pressure was 5×10^{-4} Torr.

The equilibrium shape of the epitaxial island is obtained through minimizing the total energy of the island with respect to both s and t. This gives a square island with $s = t = \alpha_0$, where the optimal size α_0 is given by:

$$\alpha_0 = e\phi h \exp\left(\frac{\Gamma}{ch}\right) \tag{5}$$

where $\Phi = e^{-3/2}\cot\theta$, e is the usual mathematical constant. The island remains square in cross section before increasing its size up to $s = t = e\alpha_0$. Due to continued oxygen exposure, the island grows beyond this critical size ($e\alpha_0$), the square shape becomes unstable and a transition to rectangular in cross section shape takes place. As the island grows further, the aspect ratio, t/s, increases, *i.e.*, reducing its width back to the optimal size, α_0, while rapidly increasing its length. In the evaluation of "c", the standard values of Young's modulus of Cu_2O (30 GPa) and shear modulus (G = 40 GPa) and Poisson ratio (ν = 0.36) of the Cu were used (Frost and Ashby, 1982; Markworth et al., 2001). The contact angle, θ = 30°, and height, h = 20 nm, were determined by the atomic force microscopy (AFM) measurement (Fig. 4b). By fitting with the critical size, $e\alpha_0$ = 114 nm, we estimated Γ from Eq. (5). Gamma (Γ) depends on the overall surface energies and interfacial energy, which are not readily available in the literature. These values were substituted into Eq. (4) to determine the energy per unit volume as a function of width s and length t. This agreement between the model and experimental observation (Fig. 4c) suggest that the oxide islands formed at this temperature have an equilibrium shape. Since the oxidation temperature is relatively high (600 °C), and the Cu surface is flat and clean, so the oxide islands can easily achieve an equilibrium shape by fast oxygen surface diffusion. This surface diffusion limited growth kinetics is also consistent with the experimentally measured volume evolution of the oxide islands (Zhou and Yang, 2002).

3.1.3.2. Cu_2O hollow pyramids. When we oxidized Cu(1 0 0) films with thickness of 700 Å at 800 °C and above, a peculiar hollow Cu_2O pyramids formed. The evolution of the island size and shape was followed within the UHV-TEM, as shown in Fig. 5a and b. The formation of terraces and empty space within the pyramid results from the sliding of an oxide segment over one another on the slip system of (1 1 1) [1 $\bar{1}$ 0] caused by the compressive stress exerted on the island due to the large volume change accompanied with oxidation of Cu to Cu_2O. The orientation of the oxide island relative to the Cu(1 0 0) was identified by selected area electron diffraction. The proposed model explains quantitatively the size distribution of the pyramid terraces. We can calculate the strain energy of an oxide island before the first slip as

$$E_s = \frac{1}{3} \times t \times \left(\frac{E}{1-\nu}\varepsilon^2\right) \times (3l^2 - 3\sqrt{2}tl + 2t^2), \tag{6}$$

where E, ν is Young's modulus and Poisson ratio of Cu_2O, respectively, $\varepsilon = (a_{Cu_2O} - a_{Cu})/a_{Cu}$ corresponds to the length constraint caused by the lattice change from Cu to Cu_2O, and l and t are the size parameters of the pyramid as defined in Fig. 5c. The oxide growth causes progressive accumulation of strain energy in the island, and the strain energy is finally released by plastic slip at some critical lateral size of the island. The work done by sliding process can be calculated as:

$$W = 3\tau \times l \times [t^2 - (t-h)^2] - \sqrt{2} \times \tau \times [t^3 - (t-h)^3] \tag{7}$$

where τ is the shear stress required for the plastic slip in the pyramid, and the size parameters are same as defined in Fig. 5c. The shear stress for the slip is estimated to be 2.5 GPa by equating Eqs. (6) and (7) and using experimentally determined width (~560 nm) and height (~55 nm) of the first terrace and ledge. The strain energy and work done by sliding for the formation of multiple terraces can be calculated similarly to determine the terrace width. Fig. 5d shows the calculated strain energy and the work done by the slip, and their intersections correspond to the island lateral size at which slips occur. The terrace widths measured from different pyramids are given in Fig. 5d, where a good agreement is noted. The above analysis suggests that the formation of the terraced hollow

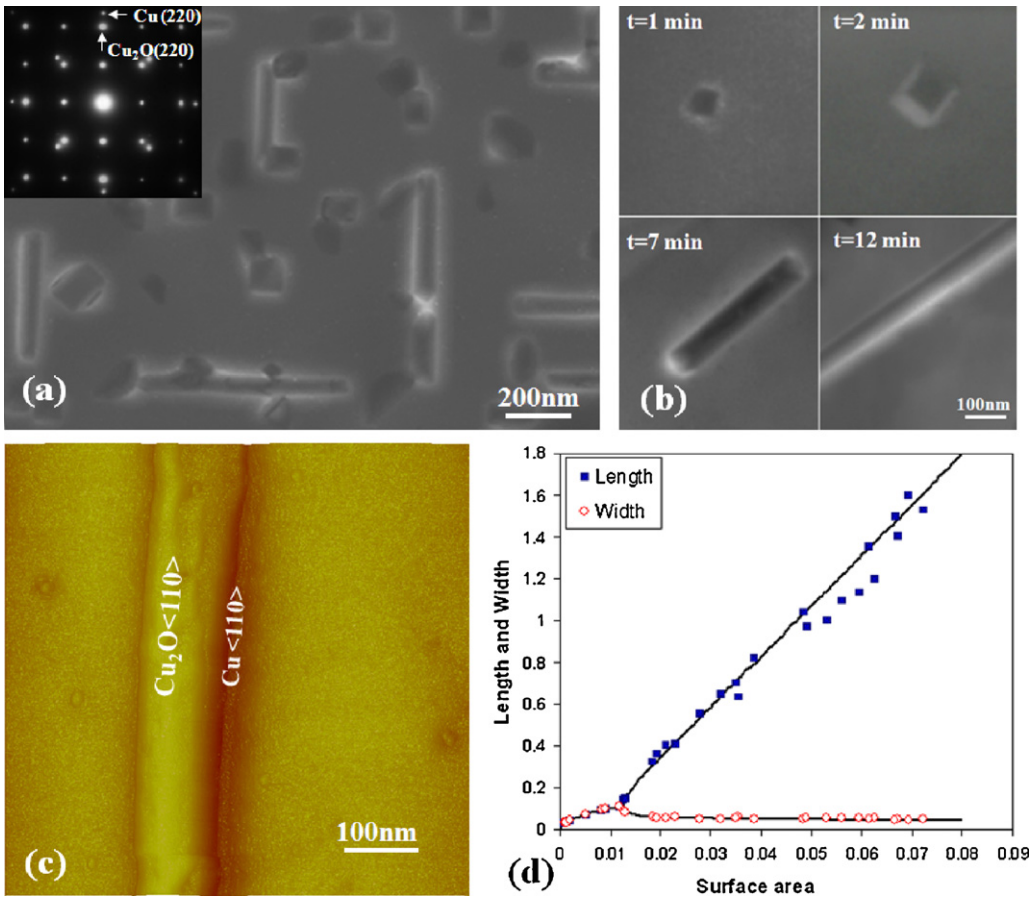

Fig. 4. (a) Cu_2O islands formed by oxidation of Cu(1 0 0) at constant oxygen partial pressure of 8×10^{-4} and temperature of 600 °C. Square shaped islands are smaller or near to the critical size of ~110 nm. Elongated islands, which have undergone shape transition, are also observed. Inset is a selected electron diffraction pattern revealing the cube-on-cube epitaxial relationship between the oxide islands and the Cu(1 0 0) substrate. The elongation directions of the islands are always along the two orientation pairs of the four crystallographic orientations, *i.e.*, ⟨1 1 0⟩ and ⟨0 $\bar{1}$ $\bar{1}$⟩ or ⟨1 $\bar{1}$ 0⟩ and ⟨$\bar{1}$ $\bar{1}$ 0⟩, and roughly equally distributed. (b) *In situ* TEM images of the four growth stages of a Cu_2O island as a function of oxidation time at constant oxygen partial pressure of 1×10^{-4} and temperature of 600 °C. The island initially has a square shape and remains a square when increasing in size, a shape transition to rectangular islands at some critical size and the aspect ratio increases with continued oxidation. The relative orientation of the oxide island to the Cu(1 0 0) film was identified by selected area electron diffraction. (c) AFM image (0.6 μm by 0.6 μm; *z* range, 0.3 μm) of an elongated Cu_2O island. (d) Dependence of both island length *t* (squares) and width *s* (circles) on the island surface area. The solid lines represent a theoretical fit based on Eq. (2). The initially square shaped island undergoes a shape transition at the critical size $s = t = e\alpha_0 = 114$ nm. There is a reduction of the width to its optimal width, α_0.

pyramids depends on the mechanical properties of the oxide and the metal films, which is temperature dependent.

3.1.4. *Effect of oxygen pressure on the orientations of oxide nuclei*

We have shown that copper and other investigators have shown on many other metals, their oxidation proceeds *via* nucleation of oxide islands (Hajcsar et al., 1995; Heinemann et al., 1975; Holloway and Hudson, 1974; Zhou, 2009a,b; Zhou and Yang, 2002, 2003b), which is assumed to have thermodynamically controlled orientations (Lawless, 1974). However, this is the case only if the metal surface is oxidized under a relatively low oxygen pressure (pO_2) as confirmed by our work presented above, and increasing the oxygen pressure will lead to nucleation of randomly oriented islands (Luo et al., 2011).

Fig. 6 shows bright-field TEM images of Cu(1 0 0) surfaces oxidized at 350 °C and different pO_2 (5×10^{-4} Torr, 0.5 Torr, and 150 Torr) for 10 min. Oxide islands are observed to form on the surface and the density of oxide nuclei increases with increasing pO_2. Selected-area electron diffraction (SAED) patterns from the oxidized surfaces reveal that Cu_2O islands nucleated under the lower pO_2 (*i.e.*, <5 Torr) have the cube-on-cube epitaxy with the Cu(1 0 0) substrate, *i.e.*, (0 1 1)Cu_2O//(0 1 1)Cu and [1 0 0]Cu_2O//[1 0 0]Cu. Oxidation at $pO_2 = 150$ Torr and above results in the nucleation of non epitaxial Cu_2O islands, as revealed by the presence of the Cu_2O diffraction ring pattern (Fig. 6c). The intensity distribution over the diffraction rings is rather uniform, suggesting that the oxide islands are oriented at random. The appearance of additional diffraction spots or rings surrounding Cu reflections in the electron diffraction patterns shown in Fig. 6 is caused by the double diffraction of Cu and Cu_2O islands. These *in situ* TEM observations indicate that the epitaxial nucleation of oxide islands cannot be maintained within the whole range of oxygen pressures. To understand this pressure-dependent orientation of oxide nuclei, we first look at the effect of oxygen pressure on the nucleation barrier for the nucleation of an oxide island on a metal surface. According to the classic heterogeneous nucleation theory, the nucleation barrier for formation of a critical oxide embryo decreases with increasing the oxygen pressure (Luo et al., 2011). At low oxygen pressure, the nucleation barrier is very high. The top priority to accelerate the nucleation kinetics is to lower the nucleation barrier. Therefore, epitaxial nucleation of oxide islands is kinetically favored. Conversely, at high oxygen pressures, the nucleation barrier is reduced and the issue of effective collisions of oxygen atoms becomes important. The nucleation of oxide islands with weak interaction and poor structural match (*i.e.*, non-epitaxial) with the metal substrate is enhanced. Kinetically speaking, in order to obtain the epitaxial oxide film on the metal substrate by oxidation, the oxygen pressure should be relatively low. If the oxygen pressure

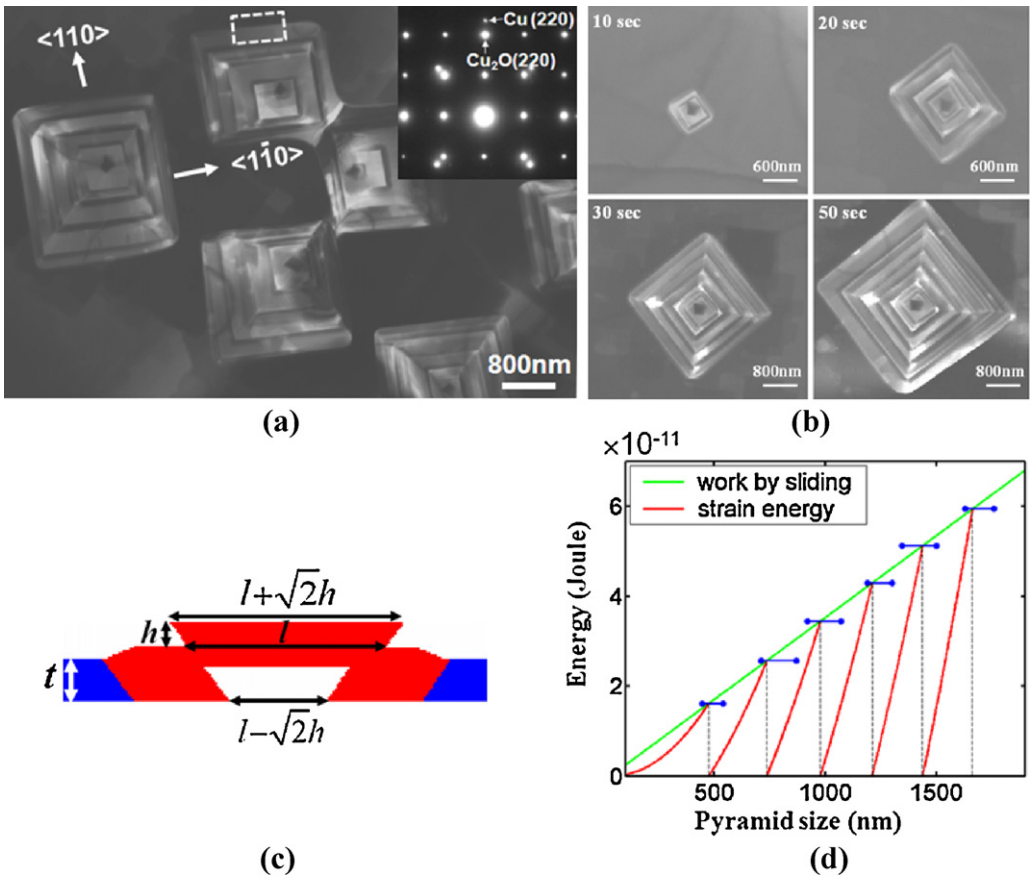

Fig. 5. (a) Typical morphology of Cu_2O terraced pyramids formed during oxidation of Cu(1 0 0) thin film at 900 °C in $pO_2 = 5 \times 10^{-4}$ Torr, inset is a selected area electron diffraction pattern from the Cu_2O/Cu interface area (dashed white rectangle) revealing the orientations of the oxide pyramid edges with respect to the Cu(1 0 0) substrate. (b) *In situ* TEM observation of the growth of a Cu_2O pyramid at 900 °C in $pO_2 = \sim 3 \times 10^{-4}$ Torr. The relative orientation was identified by selected area electron diffraction. (c) Structural parameters of the terraced pyramid; (d) plot of the strain energy and the work done by slip, where their intersections correspond to the island sizes at which plastic slips occur, the error bars represent the ranges of terrace widths obtained from experimental measurements of different pyramids.

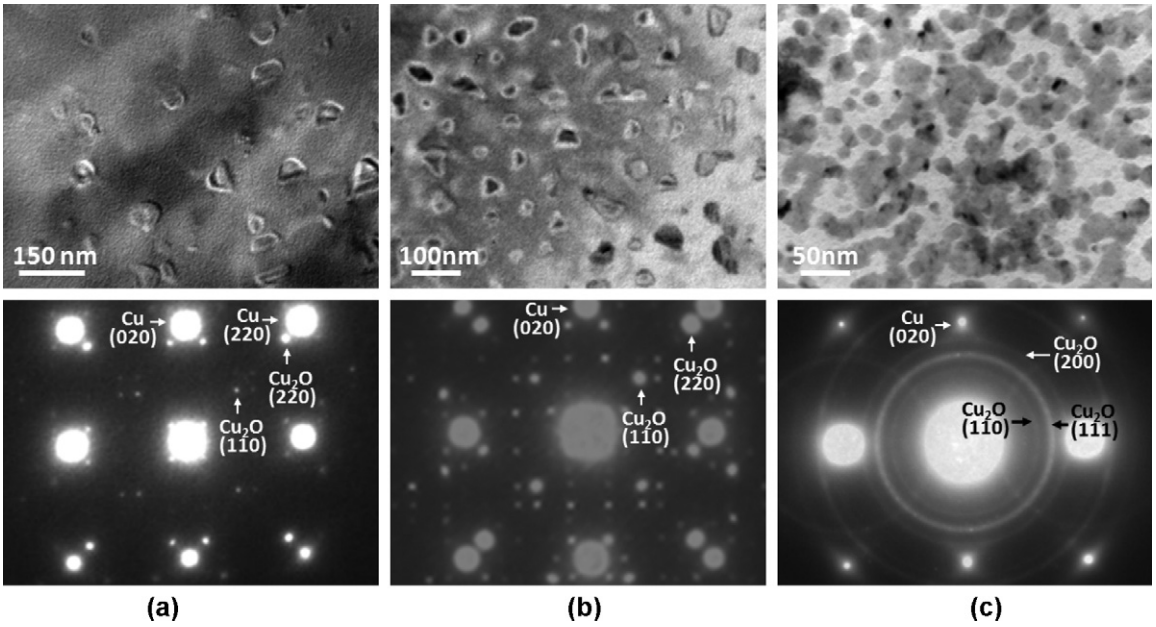

Fig. 6. (Upper panel) Bright-field TEM images of Cu_2O islands formed on Cu(1 0 0) oxidized at 350° and different oxygen pressures for 10 min, (a) $pO_2 = 5 \times 10^{-4}$ Torr, (b) $pO_2 = 0.5$ Torr, and (c) $pO_2 = 150$ Torr; (Lower panel) SAED patterns from the corresponding oxidized Cu(1 0 0) surfaces, where the additional reflections are due to double diffraction of electron beams by Cu and Cu_2O. A transition from nucleating epitaxial oxide islands to randomly oriented Cu_2O islands occurs upon increasing the oxygen pressure.

is too high, the kinetics leads to a deviation of nucleating oxide islands from the orientation of the metal substrate and the epitaxial relation will be lost. The similarity to heteroepitaxial thin film is similar to changing the deposition and temperature conditions. For low fluxes of adatoms and high temperature, the adatoms have time to migrate on the surface to find their lower (epitaxial) energy state, whereas at high flux and low temperatures, the adatoms do not have energy for migration and tend to nucleate randomly on the surface.

3.2. Atmospheric oxidation: JMAK nucleation to coalescence model

To understand oxidation under real-world conditions requires examining oxidation behavior at atmospheric pressures. Since oxidation has a long history of being investigated, classical theories of metal oxidation exist. In their classic paper of 1948, Cabrera and Mott proposed an elegant theory to explain why metals form a uniform passivation layer at low temperatures. They noted that virtually all metals show qualitatively similar behavior at low temperatures. Metals show an initially very rapid oxide growth followed by a remarkable slowing down, at some critical oxide thickness of the order of 100 Å. Since the growth of the oxide is not a thermally activated diffusion reaction at low temperatures, Cabrera and Mott proposed that the driving force is an induced electric field, which is created due to the potential difference (called the Mott Potential) of the metal/oxide work function and the oxygen/oxide work function resulting from electron tunneling between the Fermi level of the parent metal substrate and acceptor levels of chemisorbed oxygen at the oxide surface. This self-induced electric field causes an enhanced ionic transport that accelerates initial oxidation, but is rapidly attenuated with increasing thickness. When the oxide film is thick, on the order of 100 Å, then the field is no longer strong enough to induce the metal cations to migrate. Their model predicted an inverse logarithmic growth rate for metal oxides that formed due to cation diffusion outwards, *i.e.*

$$\frac{1}{X} = A - B\ln t \tag{8}$$

where X is the "thickness" of the oxide film, t is time, and A and B are fit parameters, which contain information about the energy of formation of a metal cation, the electric field and the energy barrier for diffusion across the oxide. Cabrera and Mott presented copper as one model system for passivation films formed by outward cation diffusion. Young et al. (1956) confirmed the Cabrera–Mott prediction for single crystal copper by measuring the increase of the oxide film thickness during oxidation, although they noted imperfect agreement.

A critical assumption in the Cabrera and Mott model is that the oxide film grows in a uniform layer-by-layer fashion. This cannot be confirmed by thermogravimetric data, which provides only the weight change of the material during oxidation but not structural information. In contrast, oxide island formation has been observed in several other metals and alloys. We propose a phenomenological model based on nucleation and growth, where the initial rapid oxide formation is due to oxide nucleation. Once coalescence has occurred, then a sudden reduction in the growth rate of the oxide is expected, due the change of oxidation of the surface to diffusion through an oxide layer.

Using *in situ* UHV TEM, with the Cu surface prepared *in situ* in ultrahigh vacuum, and subsequently exposed in place to high-pressure oxygen at low temperatures, we have performed experiments under identical conditions to Yang et al. (1998a, 2002) with the ability to observe microstructural details. We observed oxide island formation after exposure to 760 Torr O_2 at 70 °C for 6 min. To better visualize the oxide island nucleation and growth, we performed oxidation experiments at lower pressures, such that the kinetics were slow enough for island nucleation followed by coalescence to be readily visible. Fig. 7a–c is a sequence of dark field images when the Cu film was oxidized at 0.1 Torr and 350 °C, where coalescence to a mosaic-grained oxide film can be clearly seen. The fractional area coverage was measured from digitized micrographs using Digital Micrograph™. We find that fractional area coverage of the Cu oxide on the Cu film follows the Johnson–Mehl–Avrami–Kolmogorov (JMAK) description of the fractional coverage, $X(t)$, which has an exponential dependency on time (Avrami, 1939, 1940, 1941; Johnson and Mehl, 1939).

$$X(t) = 1 - \exp(-kt^n) \tag{9}$$

where t is time, k and n are fit parameters that depend on the surface mechanisms of transport, nucleation and growth. The parameter, n, is usually an integer or half-integer. For three-dimensional (3-D) growth, with a constant nucleation and radial growth rate, the fit parameters are $k = \pi/3$ and $n = 4$. The blue line in Fig. 7d is the best fit to the JMAK universal function of the fractional coverage: $X(t) = 1 - \exp(-kt^n)$ where $n = 2 \pm 0.005$ and $k = 1.98 \pm 2.2 \times 10^{-4}\ s^{-2}$, and the goodness of fit is $R = 0.99$.

To develop a physical model of nucleation to coalescence, we derived the fractional coverage as a function of time, following a simplified Johnson–Mehl–Avrami–Kolmogorov (JMAK) approach (Avrami, 1939, 1940, 1941; Johnson and Mehl, 1939). Given an area growth of $A(t,T)$ where t is time and T is the nucleation time and a nucleation dependency on time, $N(T)$, then the product of the derivatives, $dA(t,T)$ and $dN(T)$, will give the rate of change of the total area for all of the oxide islands prior to coalescence with neighboring islands. Once the islands start to coalesce, some island areas will be double counted. To avoid double-counting, we used the JMAK assumption that the probability of uncovered area being converted to oxide is directly proportional to the uncovered Cu surface area, $u(t)$. Then, the effective increase in the area of one island is:

$$d\Phi_1 = dA(t, T)u(t) \tag{10}$$

For the total increase in volume, the nucleation of new islands needs to be considered. The number of islands formed in a short time interval dT, at time T is $dN(T)/dT$; multiplication of Eq. (10) by $dN(T)/dT$ gives the total increase in volume of all islands due to these newly nucleated islands. Thus, the total effective 2-dimensional growth of all the islands nucleated from time $T = 0$ to $T = t$ is:

$$\frac{dX(t)}{dt} = u(t) \times \int_{T=0}^{T=t} \frac{dA(T, t)}{dt} \times \frac{dN}{dt} dT \tag{11}$$

where $X(t)$ is the fractional coverage. The fractional coverage, $X(t)$, is related to the uncovered area, $u(t)$ by: $X(t) = 1 - u(t)$, and, consequently, $dX(t)/dt = -du(t)/dt$. Expressing Eq. (11) in terms of $u(t)$ and solving for $u(t)$, we find $X(t)$:

$$X(t) = 1 - u(t) = -\exp\left\{\int\left[\int_{T=0}^{T=t} \frac{dA(T, t)}{dt} \times \frac{dN}{dt} dT\right] dt\right\} \tag{12}$$

We have previously modeled the nucleation and growth of copper oxides. The equation for two-dimensional area growth for an island that nucleated at time T (Yang et al., 1997):

$$A(t, T) = G(t - T)_{1.3} \tag{13}$$

The number of islands nucleated during a time increment dT is (Yang et al., 1998b):

$$dN(T) = k \times \exp(-k \times L_d^2 \times T) dT \tag{14}$$

We obtained the fit parameters from the analysis of the nucleation and initial growth of the copper oxide islands before coalescence,

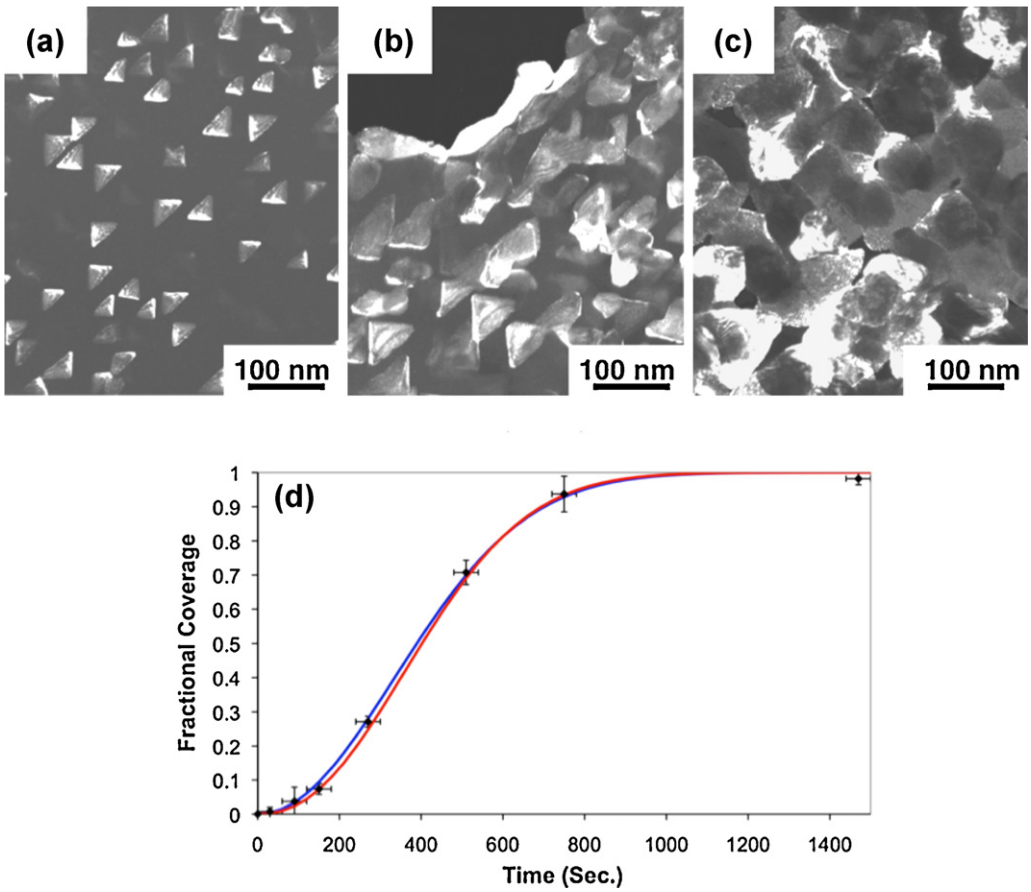

Fig. 7. Dark field images from the Cu_2O reflection showing Cu_2O island nucleation (a), growth (b) and then coalescence (c), when Cu(0 0 1) was oxidized at 0.1 Torr at 350 °C; (d) experimental data of the Cu_2O fractional area coverage, $X(t)$, *versus* time, when Cu(0 0 1) was oxidized at 0.1 Torr at 350 °C, and the comparison to the JMAK formula, $X(t) = 1 - \exp(-kt^n)$ (blue line), where $k = 1.98 \times 10^{-4}\ s^{-2}$, $n = 2$, and our derived surface model (red line) using $A(t) = Gt^{1.3}$ and $N(t) = (1/L_d^2) \times [1 - \exp(-kL_d^2 t)]$. (For interpretation of the references to color in this figure legend, the reader is referred to the web version of this article.)

to calculate the saturation density, $1/L_d^2 = 0.31209$, initial nucleation rate, $k = 2.08 \times 10^{-4}$, and the growth constant, $G = 0.00849$. Substituting the above expressions for $dN(T)$ and $dA(T)$ into Eq. (13), results in a double integral of a hypergeometric function, which was graphically solved with Mathematica™. The results of our analysis are shown in Fig. 7d where an excellent fit is noted (red line) to the experimental data (circles) (Yang et al., 2002).

We have modeled the nucleation to coalescence of copper oxides, in the framework of the JMAK equations, and noted an excellent agreement between experiment and theory, where oxygen surface diffusion is dominant. Since surface diffusion is critical, then control of the surfaces is essential in controlling oxidation properties. Extension of this surface model and experiments to atmospheric pressures and comparison to classic data could lead to a new paradigm of oxidation and passivation, where structural changes are crucial. Our results are based on *in situ* TEM of the oxidation of Cu thin films, but we suspect that these results can be generalized to other metal systems that form epitaxial oxides.

3.3. Cu alloy oxidation

Alloying commonly leads to new materials whose properties are substantially changed with respect to pure metals. For example, a general strategy for the protection of bulk metals is alloying, which leads to the formation of a uniform oxide scale layer which acts as a diffusion barrier to further oxidation attack over the alloy surface due to the preferential (selective) oxidation of one component of the alloy. The fundamental understanding of the complex atomistic mechanisms and the affects of surfaces, strain and dopants on the early stages of binary alloy oxidation will lead to smarter designs of coatings that resist oxidation as well as templates to create specific oxide nanostructures.

Binary alloy oxidation is well-described by the Wagner theory of oxidation, which predicts whether a continuous multi-layer or oxide precipitates, known as internal oxidation, form as a function of the relative amount of the added secondary element. However, this is a macroscopic description of the oxide after it has developed into a thick scale. The earlier stages of oxidation, which clearly impact the later stage oxide morphology and adhesion are not described by these classical theories. Because of the authors extensive past experience with Cu thin films, Cu–Au (Section 3.3.1) and Cu–Ni (Section 3.3.2) alloy systems were studied next, where the Cu oxidation provides a base-line for comparison. In addition to being excellent model systems, understanding the oxidation behavior of Cu-based alloys is also of practical interest. For example, Cu-based alloys are presently used as an interconnect material in electronics applications. Since materials dimensions in electronic devices are already in the nanometer regime and continually shrinking, understanding Cu alloy oxidation at the nanoscale is needed for the improved designs of durable and corrosion-resistant interconnects.

3.3.1. Cu–Au(1 0 0) oxidation

As the next simplest model system to study, we selected Cu–Au, since only Cu oxidizes. Cu and Au are 100% solid soluble at elevated temperatures. For the case of Cu–Au, only one element oxidizes (Cu). According to Vegard's law, the lattice constant of

$Cu_{1-x}Au_x$ solution is $a_{Cu_{1-x}Au_x} = a_{Au} \times x_{Au} + a_{Cu} \times (1 - x_{Au})$, where $a_{Cu} = 3.61$ Å and $a_{Au} = = 4.02$ Å, $a_{C_2O} = 4.27$ Å , and x_{Au} is mole fraction of Au in the alloy. The lattice constant of Cu–Au alloy increases with the increase of Au mole fraction and the lattice mismatch between the oxide and substrate is correspondingly reduced. The strain between the metal alloy and oxide should decrease as the Au content is increased. We noted in Section 3.1.3 that oxidation temperature influences interfacial strain that results in different oxide morphologies (*e.g.*, nanorod, hollow pyramids); thus be altering the Au content, we can systematically study strain effects on oxidation.

We find that, similar as the oxidation of Cu(1 0 0), oxide nuclei become visible on the Cu–Au surface after some incubation period, and their number increases with time and then saturates. The incubation time for the island nucleation depends on the alloy composition, higher Au mole fraction leads to longer incubation time (Zhou et al., 2007b). We speculate that Cu–Au alloys are Au rich on the surface under vacuum conditions which may be a lead to a longer incubation time as Cu diffuses to the surface when oxygen is introduced (Wang, 2005). The nucleation rate (from appearance of the first nuclei to saturation density) depends on the Au mole fraction in the alloy as well, and alloys with higher Au mole fractions exhibit faster nucleation rates (Zhou et al., 2007a). Fig. 8a shows some examples of the oxide islands formed during Cu–Au(1 0 0) oxidation at 600 °C in $pO_2 = 5 \times 10^{-4}$ Torr. Fig. 8b shows the oxide islands formed during oxidation of (1 0 0) Cu–38 at.%Au at different temperatures in $pO_2 = 5 \times 10^{-4}$ Torr. Similar to the Cu(1 0 0), the Cu_2O islands are epitaxial with the underlying alloy substrate (Zhou et al., 2006, 2007b). These measurements indicate that the saturation density depends on the oxidation temperature, *i.e.*, oxidation at a higher temperature results in a smaller number density of islands. Fig. 8a also reveals that the number density is related to the Au mole fraction in the alloys, *i.e.*, oxidation of alloys with higher Au mole fraction results in a larger saturation number density of the oxide nuclei. The activation energy for nucleation of oxide islands on the Cu–Au alloy surfaces can be deduced from the Arrhenius dependence of the saturation island density on the oxidation temperature. Fig. 8c shows the E_N values determined as a function of composition, which indicate that alloys with a larger Au mole fraction have a smaller E_N. This observation reveals that alloying Cu with Au enhances the nucleation of oxide islands. The nucleation energy of the oxide island is given by:

$$\Delta G = \Delta G^f \frac{V}{V_0} + (\gamma_0 A_0 - \gamma_m A_m + \gamma_{m/o} A_{m/o}) + \frac{E}{1-\nu}\varepsilon^2 V \qquad (15)$$

where γ are the surface and interface energies of the oxide and metal, ΔG_f is the Gibbs free energy of the oxide formation, and ε is the strain energy. With increasing Au content, the strain is reduced which may lower the nucleation energy barrier (Wang, 2005).

We also monitored the growth of oxide islands during the oxidation of CuAu(1 0 0) alloy (with 5, 10 and 15 at.% Au) at 600 °C in $pO_2 = 5 \times 10^{-4}$ Torr. The average individual island size (area) was observed to show a linear dependence on oxidation time, as shown in Fig. 8d, indicating that the growth depends on oxygen surface diffusion (Yang et al., 1997). This growth behavior is different from the oxidation of Cu(1 0 0) at 350 °C, where a slight deviation from the linear growth is noted and the non-linear oxide growth is ascribed to the oxygen surface diffusion plus oxygen direct impingement. Since the oxidation of the Cu–Au alloys is at higher temperatures, the oxygen surface diffusion can be therefore greatly enhanced. This may explain why the oxygen direct impingement is not significant in the oxide growth during the oxidation of the Cu–Au alloys at the higher temperatures. The rate constants for oxide growth, obtained from the slope of the area *vs.* time curves in Fig. 8d, decrease with increasing Au content. It is noted that alloy with a higher Au mole fraction has a smaller rate constant for oxide growth for oxidation at the same temperature, which may be due to the smaller amount of Cu available near the island.

We noted that the addition also changes the oxide morphology. Fig. 9a–c shows an *in situ* TEM observation of the growth of an oxide island formed during oxidation of Cu–5 at.%Au(1 0 0) at 600 °C and a gradual transition occurs from initially compact island shapes to a dendritic morphology as the islands grow. The oxide island nucleates with a square in cross section shape and retains this shape during the initial growth. The island then exhibit a gradual transition to a dendritic shape as growth slows along the normal to the island edges, *i.e.*, along Cu_2O ⟨1 1 0⟩ directions, while maintaining a faster growth rate along the directions of the island corners, *i.e.*, along Cu_2O ⟨1 0 0⟩ directions. In contrast, the oxide islands formed during oxidation of pure Cu(0 0 1) under the same conditions have an initially square shape that transforms to a rectangular morphology as growth proceeds (Fig. 4).

As seen from Fig. 9, a non-uniform dark contrast develops around the island with the island growth, and the energy dispersive X-ray spectroscopy (EDS) analysis reveals that the Au mole fraction is highly enhanced in the region with dark contrast (Zhou et al., 2007a). The contrast features in Fig. 9a–c reveal that the alloy film regions adjacent to the island edges become Au-rich, while there is almost no excess Au accumulation in the alloy film adjacent to the island corners, as confirmed by the EDS analysis (Zhou et al., 2007b). Fig. 9 clearly reveals that the change in the local growth rate of the island boundary is closely related to this non-uniform partition of Au atoms in the alloy film during the island growth, *i.e.*, the growth rate of the boundary adjacent to the Au-rich zone gradually slows as the local Au concentration increases.

In the initial stages of metal oxidation under low oxygen pressures and high temperatures, the reaction rate is usually dominated by the capture of oxygen. Our analysis of the growth of Cu_2O islands prior to the dendrite formation during oxidation of the Cu–Au alloys demonstrate that the rate-limiting factor controlling the oxide growth is oxygen surface diffusion. Growth of the compact shape is due to efficient diffusion of adatoms on the metal surface and along island edges (Hwang et al., 1991; Li and Evans, 2004). As oxidation progresses, a non-uniform partition of Au atoms develops in the alloy, and the local growth rate of the boundary adjacent to the Au-rich regions is slowed due to depletion of Cu atoms. As a result, the rate-limiting factor in these regions becomes Cu diffusion through the Au-rich zone, similar to reported behavior for oxidation of bulk Cu–Au alloys (Wagner, 1952). However, the growth of the dendritic tips is still controlled by fast oxygen surface diffusion because of the low Au accumulation in front of the tips. Therefore, boundary growth along the island perimeter has different rate-limiting factors that depend on the local concentration of Au in the alloy. Fig. 9d is the schematic diagram showing our proposed model of Au segregation induced dendritic growth. According to this picture, increasingly ramified morphologies are predicted as the oxidation proceeds and are also experimentally observed (Zhou et al., 2006). In comparison to Cu(0 0 1) oxidation, the addition of Au caused more rapid nucleation due to the reduced strain between the metal and the oxide but slower growth kinetics due to the Au build-up around the oxide island. The Au build up around the island also lead to a dendritic oxide growth limiting the alloy's ability to form a uniform protective oxide.

3.3.2. Cu–Ni(1 0 0) oxidation

Similar to Cu, oxidation studies of Cu–Ni alloys have a long history. Pilling and Bedworth investigated Cu–Ni oxidation by thermal gravimetric analysis to quantify the parabolic rate as function of relative concentration (Pilling and Bedworth, 1925), but these classic investigations did not provide structural information. Surface science methods, including *in situ*, examined oxygen interaction and strain induced NiO nucleation of CuNi, but focused on the

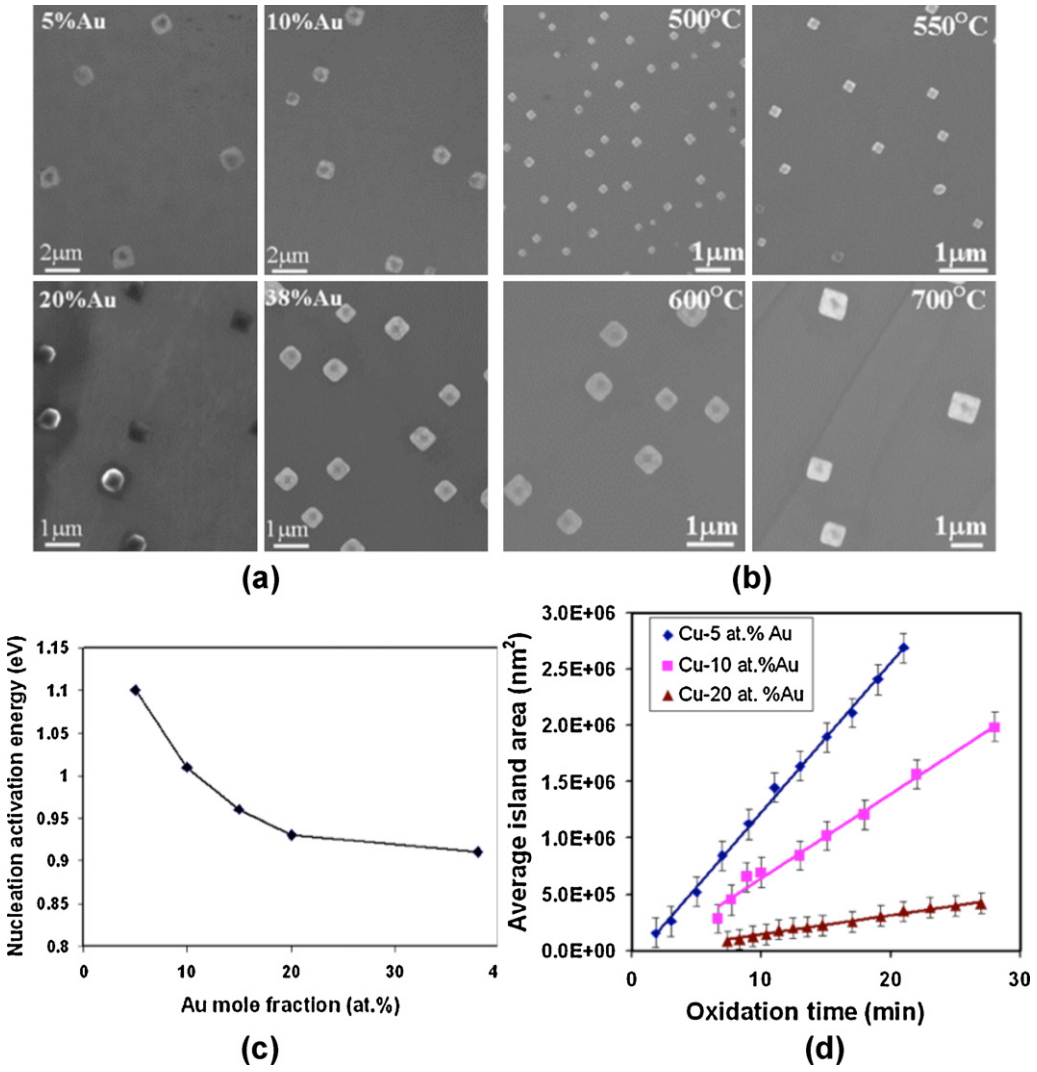

Fig. 8. (a) Bright field TEM images of oxide islands formed during oxidation of $Cu_{1-x}Au_x(1\,0\,0)$ alloys ($x = 0.05, 0.10, 0.2, 0.38$) at 600 °C and $pO_2 = 5 \times 10^{-4}$ Torr; (b) bright field TEM images of oxide islands formed during the oxidation of Cu–38 at.%Au at $pO_2 = 5 \times 10^{-4}$ Torr, but with different temperatures; (c) nucleation activation energy determined from the oxidation of the Cu–Au alloys with different Au mole fractions; (d) the average island area *vs.* oxidation time during oxidation of the Cu–Au alloys, a linear growth behavior is noted for the different alloys. The value of the slope corresponds to the rate constant for the oxide growth.

very early stages (Brizuela et al., 2006; Brueckner and Baunack, 1999; Hono et al., 1991). An *ex situ* TEM study of Cu–Ni alloy oxidation revealed that both copper oxides and nickel oxides form (Heinemann et al., 1975), but lacked temporal information needed to understand nucleation kinetics. Hence, limited literature exists for Cu–Ni oxidation studies, yet fundamental understanding of binary alloy oxidation is the critical first step to controlling selective oxidation processes.

It is reasonable to expect that the Cu–Ni alloys will show more complex behavior, since the two components are 100% solid-soluble down to ~300 °C but Cu_2O and NiO show very limited solubility. Nickel oxide, which has the cubic NaCl crystal structure, has a more negative standard free energy of formation than Cu_2O, which is simple cubic, and is expected to form more readily. In this case, depending on pO_2, either one or both components of the alloy will oxidize, thus enabling systematic determination of the effects of compositional and phase development during oxidation.

Irregular shaped oxide islands were observed to appear on Cu–24 at.%Ni(0 0 1) tens of seconds to several minutes after the introduction of oxygen gas into the TEM. This incubation time (t_o) depended on the oxidation temperature, *i.e.* $T = 500$ °C $t_o = 5$ min, $T = 600$ °C $t_o = 2$ min, and $T = 700$ °C $t_o = 40$ s, which is reasonable to expect since at higher temperatures, the barrier to nucleation can be more easily overcome due to its temperature-dependency through the corresponding Boltzmann factor. In comparison to Cu and Cu–Au oxidation, the incubation time between Cu and Cu–24 at.%Ni is quite similar, *e.g.* at $T = 600$ °C and $pO_2 = 5 \times 10^{-4}$ Torr, t_o(Cu–Ni) = 2 min, t_o(Cu) = 1.5 min and t_o(Cu–Au) = 4 min (Wang et al., 2006). We speculate that the longer incubation time before the onset of oxide nucleation for Cu–Au is due to the higher Au concentration on the surface of Cu–Au, which does not oxidize (Wang et al., 2006). The Au must migrate away from the surface as Cu migrates toward the surface as thermodynamically driven to oxidize. For Cu and Cu–Ni, the surface is already composed of elements that are thermodynamically driven to oxidize, and, hence, the oxide nucleation will occur faster in comparison to Cu–Au.

Fig. 10 are bright-field images taken *in situ* at $T = 600$ °C where the oxygen pressure is 5×10^{-4} Torr. We noted irregular-shaped elongated islands to nucleate initially, but after 15 min a second rapid nucleation stage of compact oxide islands with higher island density was observed. A similar behavior was noted at $T = 700$ °C where irregular shaped square-in-cross-section islands nucleated first, but after a couple of minutes a second nucleation of a high

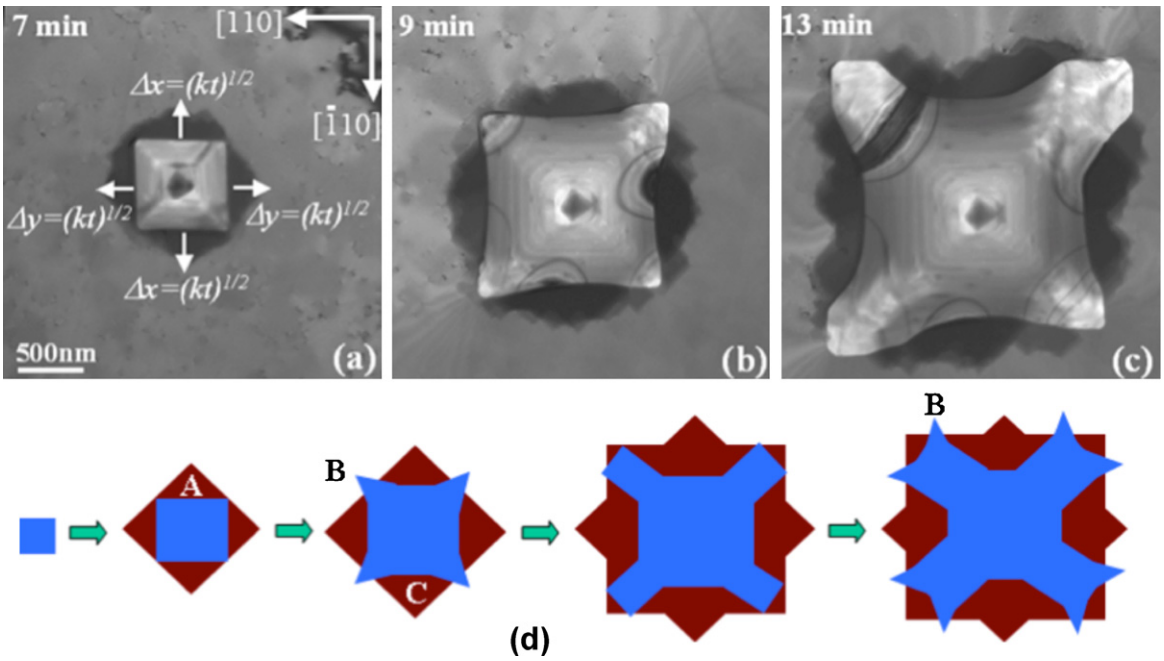

Fig. 9. (a) *In situ* TEM observation of the growth of a Cu_2O island on a Cu–5 at.%Au(1 0 0) sample at 600 °C in $pO_2 = 5 \times 10^{-4}$ Torr. A crossover from (a) an initially compact structure to (b and c) dendritic growth is observed as time progresses. The total oxidation time is noted on each image. (b) Schematics of the dendritic oxide growth in the oxidation of Cu–Au alloys, the label *A* denotes a Au-rich zone, *B* a region where growth is limited by oxygen surface diffusion, *C* a region where growth is limited by Cu diffusion through a Au-rich zone.

density of rectangular oxide islands occurred. The rapid nucleation followed by growth supports the oxide surface diffusion model where the oxidation process can be characterized by an initial nucleation rate (Yang et al., 1998b). The two-step nucleation process could be due to NiO forming first and then after the depletion of Ni, Cu_2O nucleates. The nucleation rates are 1.41 μm^{-2} min^{-1} and 0.49 μm^{-2} min^{-1} for oxidation at 600 °C and 700 °C, respectively. In comparison, the initial nucleation rates for Cu (1 0 0) at 350 °C is 0.17 μm^{-2} min^{-1} (Yang et al., 1998b) and Cu–50 at.%Au (1 0 0) oxidation at 550 °C is 7.3 μm^{-2} min^{-1} (Wang et al., 2006).

The insets in Fig. 10 are the diffraction patterns of Cu–24 at.%Ni (0 0 1) film before and after oxidation at $P(O_2) = 5 \times 10^{-4}$ Torr and $T = 600$ °C. In significant contrast to our previous results of Cu(0 0 1) (Zhou and Yang, 2005) and Cu–50 at.%Au (0 0 1) (Wang et al., 2006) where Cu_2O islands form epitaxially with a cube-on-cube orientation with respect to the underlying metal surface, these diffraction patterns reveal that polycrystalline Cu_2O and NiO oxide formed with some preferred orientations. Diffraction spots that could only be due to Cu_2O (*e.g.* Cu_2O (1 1 0)) and NiO (*e.g.* (4 0 0)NiO) were observed, demonstrating that both NiO and Cu_2O formed during *in situ* oxidation. The oxidation experiments at 500 °C and 700 °C showed similar polycrystalline oxide formation.

Polycrystalline NiO and Cu_2O formations were also noted by *in situ* synchrotron X-ray diffraction studies. *In situ* synchrotron X-ray diffraction of the initial oxidation stages of Cu–12.5 at.%Ni at $T = 450$ °C was monitored as a function of oxygen pressure, where the partial pressure of oxygen was increased from less than 10^{-10} Torr to $\sim 1 \times 10^{-5}$ Torr (Fig. 11a). Cube-on-cube oriented NiO

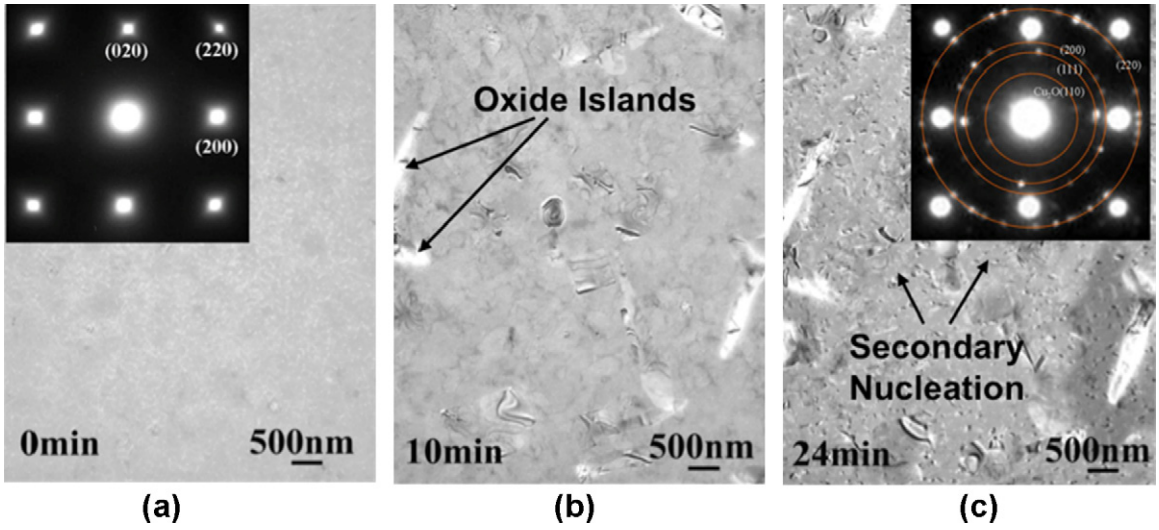

Fig. 10. Bright-field images of the *in situ* oxidation of Cu–24 at.%Ni (0 0 1) at $T = 600$ °C and $P(O_2) = 5 \times 10^{-4}$ Torr. (a) As-clean, (b) 10 min and (c) 24 min after oxygen is introduced. Insets: Selected area electron diffraction pattern of Cu–24 at.%Ni (0 0 1) film before and after oxidation at $P(O_2) = 5 \times 10^{-4}$ Torr and $T = 600$ °C, where the index (1 1 1) indicates both Cu_2O(1 1 1) and NiO(1 1 1), similarly for (2 0 0) and (2 2 0).

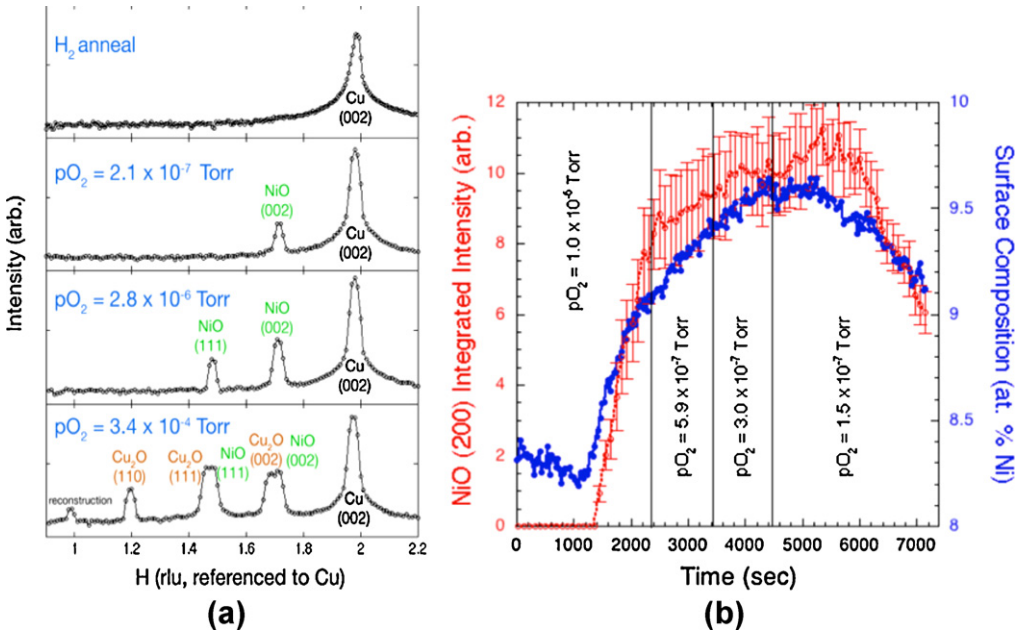

Fig. 11. (a) *In situ* synchrotron XRD patterns obtained from Cu–12.5 at.% Ni as a function of increasing oxidation partial pressure, revealing the appearance of polycrystalline NiO and then Cu_2O. Evidence of surface reconstruction appears after Cu_2O formation; (b) the appearance of the NiO diffraction peak as a function Ni surface segregation, where Ni surface segregation is correlated with the NiO nucleation, and Ni segregation away from the surface is observed to occur during NiO reduction.

forms first at $pO_2 = 2.1 \times 10^{-7}$ Torr. Increasing pO_2 led to the nucleation of other NiO epitaxial orientations, but the nucleation of NiO followed a significant incubation period. For $pO_2 \gtrsim 1 \times 10^{-4}$ Torr, which is similar to the *in situ* TEM oxidizing conditions, multiple orientations of Cu_2O also form. The distinct Cu_2O and NiO peaks are consistent with limited miscibility of Cu_2O and NiO. At $pO_2 = 3.4 \times 10^{-4}$ Torr, a (1 0 0) peak, which is possibly associated with $c(2 \times 2)$ surface structure, appeared only after Cu_2O forms.

Also, the NiO(2 0 0) diffraction peak and the surface composition of Ni, as measured by synchrotron X-ray fluorescence, were simultaneously monitored during the *in situ* oxidation and reduction of Cu–8.0 at.% Ni at $T = 450\,^{\circ}C$. The metal alloy was oxidized at 1.0×10^{-6} Torr to induce NiO formation and then the partial pressure of oxidation was gradually reduced to 1.5×10^{-7} Torr to cause NiO reduction (Fig. 11b). The surface is initially Cu-rich under vacuum conditions. Increasing pO_2 induces Ni surface segregation and NiO nucleation. Decreasing pO_2 induces NiO reduction and decreases the amount of Ni on the alloy surface. The change in the Ni surface composition is strongly correlated with NiO formation/reduction. Ongoing *in situ* investigations are being performed on this system in order to clarify the intriguing effects of temperature, pressure, composition on the selective oxidation mechanisms during the initial stages of alloy oxidation.

4. Summary

We systematically investigated the initial stages of oxidation of Cu(1 0 0), (1 1 0), and (1 1 1), and Cu–Au alloys, with relative Au compositions of 5–50 at.%, and Cu–Ni by *in situ* UHV-TEM. The main research findings for Cu oxidation is that heteroepitaxial concepts are synergistic with the initial stages of oxidation, where strain and surface structure are the critical parameters in determining oxide morphologies, thereby demonstrating a greater universality of heteroepitaxial concepts. We discovered an unusually wide variety of oxide nanostructures, from nanorods to pyramids to a nearly uniform oxide layer, by simply changing the oxidation temperature or orientation. Addition of a secondary non-oxidizing element, Au, revealed a self-limiting growth due to the depletion of Cu near the oxide island that significantly slows down the oxide growth as well as lead to an unusual dendritic shape, limiting its ability to form a uniform protective oxide. The addition of Ni altered the epitaxy from cube-on-cube to polycrystalline.

In situ UHV TEM is an ideal method to bridge the materials and (the nearly 13 orders of magnitude) pressure gap between surface science studies and bulk high and low temperature oxidation observations of real coating materials. The ability to dynamically observe the affects of thermodynamic variables, such as temperature and pressure, and materials variables, such as orientation and alloying, provided critical information in the development of a new paradigm of oxidation, where surfaces, strain and structural changes, are critical in the description of the initial oxidation behavior. Understanding the initial stages of oxidation is necessary for the predictive development of oxidation-resistant coating materials since these early stages develop into the complex oxide scale where the oxide strain determines when spallation and failure of these coating materials occur. Deeper understanding of these initial stages of oxidation will be achieved through multi-scale modeling, where recent efforts in Cu oxidation modeling have been reported (Alatalo et al., 2004; Lee and McGaughey, 2009, 2010; Liem et al., 1998, 2000). *In situ* methods are being developed rapidly to examine materials under their various oxidizing environments, including *in situ* XRD, scanning tunneling microscopy (STM), and X-ray photoelectron spectroscopy (XPS) that will also provide key insights into this critical regime of oxidation (Eastman et al., 2005; Iddir et al., 2007; Kravchuk et al., 2005; Kravchuk and Hoffman, 2006; Lahtonen et al., 2008; Lampimaki et al., 2007; Okada et al., 2007; Zhou et al., 2009). Oxidation exemplifies the fundamental materials science significantly enabled by the recent advancements with *in situ* characterization tools and theoretical simulations.

Acknowledgements

The *in situ* TEM experiments were performed at the Frederick Seitz Materials Research Laboratory, University of Illinois at Urbana-Champaign, which is supported by the U.S. Department of Energy (#DEFG02-96-ER45439). The University of Pittsburgh's work was supported by National Science Foundation (DMR

#9902863), Binghamton University's work was supported by the U.S. Department of Energy, Office of Basic Energy Sciences, Division of Materials Sciences and Engineering under Award No. DE-FG02-09ER46600. We thank J.A. Eastman for *the in situ* synchrotron X-ray diffraction study of Cu–Ni(1 0 0) oxidation, and Y. Kang for his technical assistance on the manuscript.

Appendix A. Supplementary data

Supplementary data associated with this article can be found, in the online version, at doi:10.1016/j.micron.2012.02.007.

References

Alatalo, M., Jaatinen, S., Salo, P., Laasonen, K., 2004. Oxygen adsorption on Cu(1 0 0): first-principles pseudopotential calculations. Phys. Rev. B: Condens. Matter 70, 245417.
Avrami, M., 1939. Kinetics of phase change. I: general theory. J. Chem. Phys. 7, 1103.
Avrami, M., 1940. Kinetics of phase change. II: transformation-time relations for random distribution of nuclei. J. Chem. Phys. 8, 212.
Avrami, M., 1941. Kinetics of phase change. III: granulation, phase change an microstructures. J. Chem. Phys. 9, 177.
Besenbacher, F., 1993. Oxygen chemisorption on metal surfaces: general trends for Cu, Ni and Ag. Prog. Surf. Sci. 44, 5–66.
Besenbacher, F., 1996. Scanning tunnelling microscopy studies of metal surfaces. Rep. Prog. Phys. 59, 1737–1802.
Besenbacher, F., Norskov, J.K., 1993. Oxygen chemisorption on metal surfaces: general trends for Cu, Ni and Ag. Prog. Surf. Sci. 44, 5–66.
Bharadwaj, M., Yang, J., 2001. The reduction of Cu_2O by water vapor. Scr. Mater. 44, 2557–2561.
Birks, N., Meier, G.H., 1983. Introduction to High Temperature Oxidation of Metals. Edward Arnold.
Brizuela, F., Procaccini, R., Cere, S., Vazquez, M., 2006. Anodically grown films on Cu and Cu–Ni alloys in slightly alkaline solutions. J. Appl. Electrochem. 36, 583–590.
Bruekner, W., Baunack, S., 1999. Stress and oxidation in CuNi thin films. Thin Solid Films 355, 316–321.
Brune, H., Wintterlin, J., Behm, R.J., Ertl, G., 1992. Surface migration of "hot" adatoms in the course of dissociative chemisorption of oxygen on Al(1 1 1). Phys. Rev. Lett. 68, 624–626.
Cabrera, N., Mott, N.F., 1948. Theory of the oxidation of metals. Rep. Prog. Phys. 12, 163–184.
Christensen, T.M., Raoul, C., Blakely, J.M., 1986. Change in oxide epitaxy on Ni(1 1 1): effects of oxidation temperature. Appl. Surf. Sci. 26, 408–417.
Eastman, J.A., Fuoss, P.H., Rehn, L.E., Baldo, P.M., Zhou, G.-W., Fong, D.D., Thompson, L.J., 2005. Early-stage suppression of Cu (0 0 1) oxidation. Appl. Phys. Lett. 87, 051914/1–051914/51914.
Fender, J., 1988. Fractals. New York, Plenum.
Frost, H.J., Ashby, M.F., 1982. Deformation-Mechanism Maps. Oxford, Pergamon.
Hajcsar, E.E., Underhill, P.R., Smeltzer, W.W., 1995. Initial stages of oxidation on Co–Ni alloys: island nucleation and growth. Langmuir 11, 4862–4872.
Heinemann, K., Rao, D.B., Douglas, D.L., 1975. In situ oxidation studies on (0 0 1)Cu–Ni alloy thin films. Oxid. Met. 11 (6), 321–334.
Holloway, P.H., Hudson, J.B., 1974. Kinetics of the reaction of oxygen with clean nickel single crystal surfaces. Surf. Sci. 43, 123–140.
Hono, K., Iwata, T., Nakamura, M., Pickering, H.W., Kamiya, I., Sakurai, T., 1991. Atom-probe study of the initial stage of selective oxidation of Ni from the Cu–Ni alloy system. Surf. Sci. 245, 132–149.
Hwang, R.Q., Schroder, J., Gunther, C., Behm, R.J., 1991. Fractal growth of two-dimensional islands: Au on Ru(0 0 0 1). Phys. Rev. Lett. 67, 3279–3282.
Iddir, H., Fong, D.D., Zapol, P., Fuoss, P.H., Curtiss, L.A., Zhou, G.-W., Eastman, J.A., 2007. Order-disorder phase transition of the Cu(0 0 1) surface under equilibrium oxygen pressure. Phys. Rev. B: Condens. Matter 76, 241401–241404.
Jacobsen, J., Hammer, B., Jacobsen, K.W., Nørskov, J.K., 1995. Electronic structure, total energies, and STM images of clean and oxygen-covered Al (1 1 1). Phys. Rev. B 52, 14954–14962.
Jacobsen, K.W., Norskov, J.K., 1990. Theory of the oxygen-induced restructuring of Cu(1 1 0) and Cu(1 0 0) surfaces. Phys. Rev. Lett. 65, 1788.
Jenkins, S.J., 2006. Dissociative adsorption and adsorbate-induced reconstruction on Fe{2 1 1}. Surf. Sci. 600 (7), 1431–1438.
Jensen, F., Besenbacher, F., Lagsgaard, E., Stensgaard, I., 1990. Dynamics of oxygen-induced reconstruction of Cu(1 0 0) studied by scanning tunneling microscopy. Phys. Rev. B 42, 9206–9209.
Jensen, F., Besenbacher, F., Lagsgaard, E., Stensgaard, I., 1991. Oxidation of Cu(1 1 1): two new oxygen induced reconstructions. Surf. Sci. 259, L774–L780.
Jensen, F., Besenbacher, F., Stensgaard, I., 1992. Two new oxygen induced reconstructions on Cu(1 1 1). Surf. Sci. 269/270, 400–404.
Johnson, W.A., Mehl, R., 1939. Reaction kinetics in processes of nucleation and growth. Trans. AIME 135, 415.
Kennett, H.M., Lee, A.E., 1975. The initial oxidation of molybdenum V. A model for the nucleation of epitaxial oxide and its application to molybdenum. Surf. Sci. 48, 633–648.
Kravchuk, T., Akhvlediani, R., Hoffman, A., 2005. Surface and sub-surface oxidation of Cu-(17 at.%)Al(1 0 0) studied by X-ray photo-electron spectroscopy and low energy He^+ scattering spectroscopy. Nucl. Instrum. Methods Phys. Res., Sect. B. 230, 413–418.
Kravchuk, T., Hoffman, A., 2006. Enhanced reactivity and selectivity in oxidation of Cu(1 0 0) and α-Cu–Al(5 at.%) (1 0 0) surfaces studied by electron and ion spectroscopies. Surf. Sci. 600 (6), 1252–1259.
Lahtonen, K., Hirsimäki, M., Lampimäki, M., Valden, M., 2008. Oxygen adsorption-induced nanostructures and island formation on Cu(1 0 0): bridging the gap between the formation of surface confined oxygen chemisorption layer and oxide formation. J. Chem. Phys. 129, 124703.
Lampimaki, M., Lahtonen, K., Hirsimaki, M., Valden, M., 2007. Oxidation-induced nanostructures on Cu{1 0 0}, Cu(Ag) and Ag/Cu{1 0 0} studied by photoelectron spectroscopy. Surf. Interface Anal. 39 (4), 359–366.
Lawless, K., Mitchell, D., 1965. The oxidation of copper single crystals. Mem. Sci. Rev. Metall. LXII, 17–45.
Lawless, K.R., 1974. The oxidation of metals. Rep. Prog. Phys. 37, 231–316.
Lee, M., McGaughey, A.J.H., 2009. Energetics of oxygen embedment into unreconstructed and reconstructed Cu(1 0 0) surfaces: density functional theory calculations. Surf. Sci. 603 (24), 3404–3409.
Lee, M., McGaughey, A.J.H., 2010. Role of sub-surface oxygen in Cu(1 0 0) oxidation. Surf. Sci. 604 (17–18), 1425–1431.
Li, M.Z., Evans, J.W., 2004. Growth coalescence shapes for islands during metal (1 0 0) homoepitaxy. Phys. Rev. B 69, 035410.
Liem, S.Y., Clarke, J.H.R., Kresse, G., 2000. Pathways to dissociation of O_2 on Cu(1 1 0) surface: first principles simulations. Surf. Sci. 459, 104–114.
Liem, S.Y., Kresse, G., Clarke, J.H.R., 1998. First principles calculation of oxygen adsorption and reconstruction of Cu(1 1 0) surface. Surf. Sci. 415, 194–211.
Luo, L., Kang, Y., Liu, Z., Yang, J.C., Zhou, G., 2011. Dependence of degree of orientation of copper oxide nuclei on oxygen pressure during initial stages of copper oxidation. Phys. Rev. B. 83 (15), 155418.
Markworth, P.R., Liu, X., Dai, J.Y., Fan, W., Marks, T.J., Chang, R.P.H., 2001. J. Mater. Res. 16, 2408–2414.
Matsumoto, T., Bennett, R.A., Stone, P., Yamada, T., Domen, K., Bowker, M., 2001. Scanning tunneling microscopy studies of oxygen adsorption on Cu(1 1 1). Surf. Sci. 471 (1–3), 225–245.
McDonald, M.L., Gibson, J.M., Unterwald, F.C., 1989. Design of an ultrahigh-vacuum specimen environment for high-resolution transmission electron microscopy. Rev. Sci. Instrum. 60 (4), 700–707.
Milne, R.H., Howie, A., 1984. Electron microscopy of copper oxidation. Philos. Mag. A 49 (5), 665–682.
Okada, M., Vattuone, L., Moritani, K., Savio, L., Teraoka, Y., Kasai, T., Rocca, M., 2007. X-ray photoemission study of the temperature-dependent CuO formation on Cu(4 1 0) using an energetic O-2 molecular beam. Phys. Rev. B: Condens. Matter 75 (23), 4.
Orr, W.H., 1962. Oxide Nucleation and Growth. Cornell University, Ithaca, NY.
Pilling, N., Bedworth, R., 1925. Oxidation of copper-nickel at high temperatures. Ind. Eng. Chem. 17 (4), 372–376.
Qin, F., Anderegg, J.W., Jenks, C.J., Gleeson, B., Sordelet, D.J., Thiel, P.A., 2008. X-ray photoelectron spectroscopy studies of the early-stage oxidation behavior of (Pt, Ni)3Al(1 1 1) surfaces in air. Surf. Sci. 602 (1), 205–215.
Robinson, I.K., Vlieg, E., Ferrer, S., 1990. Oxygen-induced missing-row reconstruction of Cu(0 0 1) and Cu(0 0 1)-vicinal surfaces. Phys. Rev. B 42, 6954.
Ross, F.M., Tersoff, J., Tromp, R.M., 1998. Coarsening of self-assembled Ge quantum dots on Si(0 0 1). Phys. Rev. Lett. 80 (5), 984.
Ross, F.M., Tromp, R.M., Reuter, M.C., 1999. Transition states between pyramids and domes during Ge/Si island growth. Science 286, 1931–1934.
Stauffer, D., 1979. Scaling theory of percolation clusters. Phys. Rep. 54 (1), 1–71.
Tersoff, J., LeGoues, F.K., 1994. Competing relaxation mechanisms in strained layers. Phys. Rev. Lett. 72, 3570.
Tersoff, J., Tromp, R.M., 1993. Shape transition in growth of strained islands: spontaneous formation of quantum wires. Phys. Rev. Lett. 70, 2782–2785.
Thurmer, K., Williams, E., Reutt-Robey, J., 2002. Autocatalytic oxidation of lead crystallite surfaces. Science 297, 2033–2035.
Tromp, R.M., Ross, F.M., 2000. Advances in situ ultra-high vacuum electron microscopy: growth of SiGe on Si. Annu. Rev. Mater. Sci. 30, 431–449.
Vaquila, I., Passeggi, M., Ferron, J., 1993. Oxide stoichiometry in the early stages of titanium oxidation at low pressure. J. Phys.: Condens. Matter 5, A157–A158.
Wagner, C., 1933. Beitrag zur theorie des anlaufvorgangs. Z. Phys. Chem. B 21, 25–41.
Wagner, C., 1952. Theoretical analysis of the diffusion processes determining the oxidation rate of alloys. J. Electrochem. Soc. 99 (10), 369–380.
Wang, L., 2005. Dynamic Investigation of Cu50Au(0 0 1) Alloy Nano-oxidation by In Situ UHV-TEM. Materials Science and Engineering, University of Pittsburgh, Pittsburgh, pp. 1–62.
Wang, L., Zhou, G.W., Eastman, J., Yang, J.C., 2006. Initial oxidation kinetics and energetics of Cu0 5Au0.5 (0 0 1) film investigated by in situ ultrahigh vacuum transmission electron microscopy. Surf. Sci. 600, 2372–2378.
Yagyu, K., Liu, X., Yoshimoto, Y., Nakatsuji, K., Komori, F., 2009. Dissociative adsorption of oxygen on clean Cu(0 0 1) surface. J. Phys. Chem. C 113 (14), 5541–5546.
Yang, J.C., Kolasa, B., Gibson, J.M., Yeadon, M., 1998a. Self-limiting oxidation of copper. Appl. Phys. Lett. 73, 2841–2843.
Yang, J.C., Li, Z., Sun, L., Zhou, G., Eastman, J.A., Fong, D.D., Fuoss, P.H., Baldo, P.M., Rehn, L.E., Thomson, L.J., 2009. Polycrystalline oxides formation during transient oxidation of (0 0 1)Cu–Ni binary alloys studied by *in situ* TEM and XRD. Mater. High Temp. 28 (1), 1–8.

Yang, J.C., Tropia, L., Evan, D., 2002. From nucleation to coalescence of Cu_2O islands during *in situ* oxidation of Cu(0 0 1). Appl. Phys. Lett. 81, 241–243.
Yang, J.C., Yeadon, M., 1997. Oxygen surface diffusion in three-dimensional Cu_2O growth on Cu(0 0 1) thin films. App. Phys. Lett. 70 (26), 3522–3524.
Yang, J.C., Yeadon, M., Kolasa, B., Gibson, J.M., 1997. Oxygen surface diffusion in 3-d Cu_2O growth on Cu(0 0 1) thin films. Appl. Phys. Lett. 70 (26), 3522–3524.
Yang, J.C., Yeadon, M., Kolasa, B., Gibson, J.M., 1998b. Homogeneous nucleation of Cu_2O on (0 0 1)Cu. Scr. Mater. 38 (8), 1237–1242.
Yang, J.C., Yeadon, M., Kolasa, B., Gibson, J.M., 1998c. In situ UHV TEM investigations of the initial oxidation stage of copper thin films. MRS Proc. 481, 557–562.
Yang, J.C., Yeadon, M., Kolasa, B., Gibson, J.M., 1999. The limited role of surface defects as nucleation sites for Cu_2O on Cu(0 0 1). J. Electrochem. Soc. 146, 2103–2106.
Young, F., Cathcart, J., Gwathmey, A., 1956. The rates of oxidation of several faces of a single crystal of copper as determined with elliptically polarized light. Acta Metall. 4, 145–152.
Zhou, G.W., 2009a. Nucleation thermodynamics of oxide during metal oxidation. Appl. Phys. Lett. 94, 201905/1–201905/201905.
Zhou, G.W., 2009b. Stress-driven formation of terraced hollow oxide nanorods during metal oxidation. J. Appl. Phys. 105 (10), 104302–104306.
Zhou, G.W., 2009c. TEM investigation of interfaces during cuprous island growth. Acta Mater. 57 (15), 4432–4439.
Zhou, G.W., 2010. Nucleation-induced kinetic hindrance to the oxide formation during the initial oxidation of metals. Phys. Rev. B. 81 (19), 195440–195441–195447.
Zhou, G.W., Chen, X., Gallagher, D., Yang, J.C., 2008. Percolating oxide film growth during Cu(1 1 1) oxidation. Appl. Phys. Lett. 93, 123104–123106.
Zhou, G.W., Eastman, J.A., Birtcher, R.C., Pearson, J.E., Baldo, P.E., Thompson, L.J., 2007a. Composition effects on the early-stage oxidation kinetics of (0 0 1)Cu–Au alloys. J. Appl. Phys. 101, 033521/1–033521/33521.
Zhou, G.W., Fong, D.D., Wang, L., Fuoss, P.H., Baldo, P.M., Thompson, L.J., Eastman, J.A., 2009. Nanoscale duplex oxide growth during early stages of oxidation of Cu–Ni(1 0 0). Phys. Rev. B: Condens. Matter 80 (13), 134106/1–134106/134106.
Zhou, G.W., Slaughter, W.S., Yang, J.C., 2005a. Terraced hollow oxide pyramids. Phys. Rev. Lett. 94, 246101–246104.
Zhou, G.W., Wang, L., Yang, J.C., 2005b. Effect of surface topology on the formation of oxide islands on Cu surfaces. J. Appl. Phys. 97, 063509/1–063509/63509.
Zhou, G.W., Wang, L., Birtcher, R.C., Baldo, P.E., Pearson, J.E., Yang, J.C., Eastman, J.A., 2006. Cu_2O island shape transition during Cu–Au oxidation. Phys. Rev. Lett. 96, 226108–226111.
Zhou, G.W., Wang, L., Birtcher, R.C., Baldo, P.M., Pearson, J.E., Yang, J.C., Eastman, J.A., 2007b. Effect of composition on the early-stage oxidation of (1 0 0)Cu–Au alloys. J. Appl. Phys. 101, 033521–033526.
Zhou, G.W., Yang, J.C., 2002. Formation of quasi one-dimensional Cu_2O structures by in situ oxidation of Cu(0 0 1). Phys. Rev. Lett. 89, 106101–106104.
Zhou, G.W., Yang, J.C., 2003a. Initial oxidation kinetics of copper (1 1 0) film investigated by *in situ* UHV-TEM. Surf. Sci. 531, 359–367.
Zhou, G.W., Yang, J.C., 2003b. Temperature effect on the Cu_2O oxide morphology created by oxidation of Cu(0 0 1) as investigated by *in situ* UHV-TEM. Appl. Surf. Sci. 210, 165–170.
Zhou, G.W., Yang, J.C., 2004. Temperature effects on the growth of oxide islands on Cu (1 1 0). Appl. Surf. Sci. 222, 357–364.
Zhou, G., Yang, J.C., 2005. Initial oxidation kinetics of Cu(1 0 0), (1 1 0), and (1 1 1) thin films investigated by *in situ* UHV-TEM. J. Mater. Res. 20 (7), 1684–1694.
Zhukov, V., Popova, I., Yates, J.T., 1999. Initial stages of Al(1 1 1) oxidation with oxygen temperature dependence for the integral reactive sticking coefficient. Surf. Sci. 441 (2–3), 251–264.